GEOMETRY OPTIMIZATION WITH VARIATIONALLY CONSISTENT FORCES USING HIGHER-ORDER FINITE ELEMENT METHODS IN KOHN-SHAM DENSITY FUNCTIONAL THEORY CALCULATIONS

A THESIS SUBMITTED TO

THE GRADUATE SCHOOL OF ENGINEERING AND SCIENCE

OF BILKENT UNIVERSITY

IN PARTIAL FULFILLMENT OF THE REQUIREMENTS FOR

THE DEGREE OF

MASTER OF SCIENCE

IN

MECHANICAL ENGINEERING

By

Kaan Karaca

September 2021

GEOMETRY OPTIMIZATION WITH VARIATIONALLY CONSISTENT FORCES USING HIGHER-ORDER FINITE ELEMENT METHODS IN KOHN-SHAM DENSITY FUNCTIONAL THEORY CALCULATIONS

By Kaan Karaca

September 2021

We certify that we have read this thesis and that in our opinion it is fully adequate, in scope and in quality, as a thesis for the degree of Master of Science.

İlker Temizer(Advisor)

Oğuz Gülseren

Hande Toffoli

Approved for the Graduate School of Engineering and Science:

Ezhan Karaşan
Director of the Graduate School

ABSTRACT

GEOMETRY OPTIMIZATION WITH VARIATIONALLY CONSISTENT FORCES USING HIGHER-ORDER FINITE ELEMENT METHODS IN KOHN-SHAM DENSITY FUNCTIONAL THEORY CALCULATIONS

Kaan Karaca
M.S. in Mechanical Engineering
Advisor: İlker Temizer
September 2021

Variationally consistent atomic forces are computed for Kohn-Sham density functional theory (DFT) solved via a higher order finite element (FEM) framework. Force expressions are derived for pseudopotential and all-electron settings in a unified structure. Generalized gradient approximations are additionally addressed together with nonlinear core correction in the same pseudopotential setting. Classical Lagrange basis functions are used as well as non-uniform rational B-spline (NURBS) basis in isogeometric analysis concept. Calculated forces have been shown to be variationally consistent with energies. Reference force values have been generated through Kohn-Sham DFT software packages and accuracy of forces is verified. Finally, geometry optimizations have been conducted. For this purpose, several optimization algorithms are tested for their robustness, computational cost and ease of implementation. Fast inertial relaxation engine (FIRE) algorithm is eventually chosen as the optimization algorithm. Variationally consistent forces allow conducting geometry optimization even at coarse meshes, finding the energy minima of any particular setup. Optimized ground state geometries have also been compared with those obtained from reference software packages, showing very close agreement with values reported in literature.

Keywords: Kohn-Sham density functional theory, finite element method, isogeometric analysis, force calculation, geometry optimization.

ÖZET

YÜKSEK DERECELİ SONLU ELEMANLAR YÖNTEMİ TABANLI KOHN-SHAM YOĞUNLUK FONKSİYONEL KURAMI ÇERÇEVESİNDE VARYASYONEL TUTARLI KUVVETLERLE GEOMETRİ ENİYİLEMESİ

Kaan Karaca
Makine Mühendisliği, Yüksek Lisans
Tez Danışmanı: İlker Temizer
Eylül 2021

Varyasyonel olarak tutarlı atomik kuvvetler yüksek dereceli sonlu elemanlar yöntemi ile çözülen Kohn-Sham yoğunluk fonksiyonel (YFK) kuramı yapısında hesaplanmıştır. Kuvvet ifadeleri tüm-elektron ve pseudo-potansiyel uygulamaları için tek bir yapıda türetilmiştir. Bununla beraber, genelleştirilmiş gradyan fonksiyoneli (GGA), doğrusal olmayan çekirdek düzeltmesi (NLCC) ile aynı pseudo-potantiyel formülasyonunda ele alınmıştır. Klasik Lagrange taban fonksiyonlarının yanı sıra izogeometrik analiz anlayışı içerisinde düzgün olmayan rasyonel temelli eğri (NURBS) taban fonksiyonları da kullanılmıştır. Hesaplanan kuvvetlerin enerjiyle varyasyonel tutarlı olduğu gösterilmiştir. Kohn-Sham YFK yazılımsal paketlerinden referans kuvvetleri elde edilmiş ve kuvvetlerin doğruluğu kanıtlanmıştır. Son olarak, geometri eniyilemesi gerçekleştirilmiştir. Bu amaçla, farklı eniyileme algoritmaları sağlamlık, hesap değeri ve uygulama kolaylığı için denenmiştir. Sonuç olarak hızlı ataletsel gevşeme motoru (FIRE) algoritması eniyileme algoritması olarak seçilmiştir. Varyasyonel tutarlı kuvvetler düşük çözünürlüklü ağlarda bile geometri eniyilemesi yapma imkanı sunarak herhangi bir ağın minumum enerji değerini bulabilir. Eniyilenen temel durum geometrileri yazılımsal paketlerden elde edilen referans değerlerle karşılaştırılmış, literatürde sunulan sonuçlara çok yakın olarak uydukları görülmüştür.

Anahtar sözcükler: Kohn-Sham yoğunluk fonksiyonel kuramı, sonlu elemanlar yöntemi, izogeometrik analiz, kuvvet hesabı, geometri eniyilemesi.

Acknowledgement

I would like thank my advisor Dr. İlker Temizer for this opportunity. This work was made possible thanks to his patience and guidance for the last three years.

I want to express my sincerest gratitude to my family for years of endless love and support. Needless to say, you have always been the core of my life, I would not have the joy and determination without having your support all my life.

Support by the Scientific and Technological Research Council of Turkey (TÜBİTAK) under the 1001 Programme (Grant No: 119M981) is also kindly acknowledged.

Contents

List of Figures

List of Tables

Chapter 1

Introduction

One of the major goals of electronic structure calculation is energy calculation. Nevertheless, many other material properties can be obtained through electronic structure calculation and are under significant investigation as well [1]. Hartree-Fock method [2] and Kohn-Sham density functional theory [3] are two of the most well-known calculation methods for these investigations. Whatever the method is, a discretization scheme is constructed to solve the relevant equations via the implementation of a basis set. Traditionally, Gaussian basis sets [4] have been applied for all-electron problems, whereas planewaves [5], good at representing periodicity, have been popularized for pseudopotential calculations. Although popular, both methods have their drawbacks, such as incompleteness of Gaussian basis sets leading to non-systemic convergence and lack of local refinement capability for planewaves. Finite element method, on the other hand, accounts for these drawbacks, with its local refinement capability and locally supported basis functions and it has been long implemented [6] for Kohn-Sham DFT. Additionally, FEM offers systematic improvement in energy calculation with refinement while respecting the variational nature of the problem [7]. Recently, regarding FEM based solutions, generalized gradient correction exchange correlation (GGA) functional along with nonlinear core correction (NLCC) has also been implemented [8, 9] in several works that previously featured only local density approximation (LDA) assumption [10, 11].

Along with energy, atomic forces are a major quantity of interest in electronic structure calculations, since they are employed in deciding the equilibrium geometry. Atomic forces are famously calculated using the Hellmann-Feyman theorem [12], which reduces the atomic force expression to only electrostatic interaction terms. Nevertheless, implementation of Hellmann-Feyman theorem forces has remained tricky, as Pulay forces [13] usually occur with many discretizations and basis sets. Previously, force calculations have been performed using planewaves [14, 15] and Gaussian type basis sets [16, 17] in accordance with Hellmann-Feyman theorem. Mixed Gaussian-planewave basis set approach [18, 19] was also proved viable for force calculation where calculated forces have been used towards molecular dynamics [18].

Hellmann-Feyman theorem has also been applied in other real space methods in the context of DFT. In an orbital-free and another Kohn-Sham DFT formulation solved via finite difference method, pseudopotential force calculations required taking the overlapping nuclear density into account whenever pseudocharges are significantly close to each other [20, 21], whereas an additional nonlocal pseudopotential force term was sufficient to express the forces calculated via a discontinuous Galerkin formulated Kohn-Sham DFT solution [22].

Hellman-Feymann forces have also been implemented in FEM based Kohn-Sham DFT [23]. Based on the FEM discretization, force expression has been showed to deviate from the classic Hellman-Feynman force to account for the mesh induced force effects [23]. Moreover, configurational force approach [24, 8] is also introduced recently, citing the problems arising with Hellmann-Feyman theorem such as Pulay forces and failure to predict stress in periodic setting [25].

Convergence of forces through refinement has been investigated in several studies as well. Galerkin formulated Kohn-Sham DFT solution [22] reports systematic convergence of forces along with energy without discussing convergence rates. Finite difference methods employed in orbital-free DFT and Kohn-Sham DFT both record systematic convergence as well, yet while Kohn-Sham DFT method [21] presented similar convergence rates for energy and forces, in orbital-free DFT

method [20] convergence rates of forces have surpassed those of energies. Configurational force approach in Kohn-Sham DFT [24] on the other hand achieved approximately one order less convergence rates for forces than those of energies.

A major concern of error in force calculation is egg-box effect, a phenomenon observed as oscillations in energy and forces upon translating the molecule in a mesh that does not feature translational invariance property [26, 27, 28, 29]. This effect is detrimental to efficient geometry optimization. Several suggestions have been put forward to mitigate this effect. One suggestion is the manipulation of psedupotential projector functions through Fourier filtering [27, 28] and efficient grid construction [28]. Also, using derivatives of wavefunctions instead of potentials for force calculations in suitable cases where wavefunctions behave smoother has been invoked [27]. Finally, egg-box effect has been observed to diminish through refinement [26] such as decreasing the grid spacing or increasing the energy cut-off radius in applicable cases. In order to ease performing geometry optimization as well as molecular dynamics under egg-box effect, a modified force approach [30] has also been proposed where calculated forces are altered based on atomic positions by preserving the initial center of mass of the system. Nevertheless, geometry optimization still remains a difficult task in the presence of strong egg-box effects.

Finally, with nonlocal pseudopotentials, where the pseudopotential, hence the force, terms are expressed using multiple functions, it has been showed that force term arising from nonlocal contribution can be expressed using the gradient of the wavefunctions instead of the gradient of nonlocal potential with small error in calculations [31].

Goal of this work is to form a unified variationally consistent force expression for all-electron and pseudopotential formulations with both LDA and GGA+NLCC capability for Kohn-Sham DFT solved within a FEM framework, where variationally consistent forces are subsequently to be used in geometry optimization. In Chapter 2, Kohn-Sham DFT problem is introduced together with the corresponding electrostatic problem. Implementation within the FEM framework is explained by reformulating the problem statements for the FEM concept.

Mesh construction is briefly discussed. Chapter 3 continues with the derivation of force expressions and argues their variational consistency. In Chapter 4 and Chapter 5, calculated force results for pseudopotential and all-electron settings are presented respectively, with a strong emphasis on pseudopotential calculations in view of the fixed mesh. Finally, Chapter 6 discusses the geometry optimization scheme, and presents results for geometry optimizations conducted with variationally consistent forces. Note that force calculation and geometry optimization capabilities to be discussed and exemplified in this work have been implemented within a previously developed FEM-based Kohn-Sham DFT framework [9, 10].

Chapter 2

Electronic structure formulation

2.1 Non-relativistic time-independent Schrödinger equation

Quantum mechanical electronic structure of materials is principally decided by solving the Schrödinger equation [32], or more specifically non-relativistic time-independent Schrödinger equation if such dependencies are not investigated as in the case of this thesis. Schrödinger equation is in the form of an eigenvalue problem, and its solution results in electronic wavefunctions (Ψ) as the eigenvectors and electronic energy (E) as the eigenvalues:

$$\hat{H}\Psi = E\Psi \tag{2.1}$$

Hamiltonian $\hat{H}$ is called the electronic Hamilton if it lacks the nuclear kinetic energy and nucleus-nucleus interaction energy contributions. Electronic Hamiltonian more specifically can be expanded as

$$\hat{H} = \hat{T} + \hat{E}_{ne} + \hat{E}_{ee} \tag{2.2}$$

where $\hat{T}$, $\hat{E}_{ee}$ and $\hat{E}_{ne}$ denote kinetic, electron-electron interaction and electron-nucleus interaction energies respectively. For a system consisting of N electrons

and M nuclei, resultant electronic Hamiltonian in (2.2) has the components

$$\hat{T} = \sum_{i=1}^{N}(-\frac{1}{2}\nabla_i^2) \ , \quad \hat{E}_{ne} = \sum_{i=1}^{N} v_{ext}(\boldsymbol{r}_i) \ , \quad \hat{E}_{ee} = \sum_{i=1}^{N}\sum_{j>i}^{N} \frac{1}{r_{ij}} \tag{2.3}$$

where v_{ext} is the external potential acting on the electron i, and r_{ij} is the distance between the spatial positions of electrons i and j ($\boldsymbol{r}_i$ and $\boldsymbol{r}_j$ respectively). Throughout this work, v_{ext} will only consist of the nuclear potential, thus v_{ext} can be expanded further into individual nucleus contributions as

$$v_{ext}(\boldsymbol{r}) = \sum_{A=1}^{M} v_A(\boldsymbol{r}), \qquad v_A(\boldsymbol{r}) = -\frac{Z_A}{|\boldsymbol{r} - \boldsymbol{R}_A|} \tag{2.4}$$

where $\boldsymbol{R}_A$ is the position of nucleus A. If the total energy of the system is to be defined, nucleus-nucleus interaction energy and nuclear kinetic energy must be added to electronic energy. However, since nuclear velocities are negligible in comparison to electronic velocities, due to Born-Oppenheimer approximation [2] nuclear kinetic energy is omitted, and the Hamiltonian is defined for static nuclei. Therefore, only nucleus-nucleus interaction energy is additionally needed:

$$E_{nn} = \sum_{A=1}^{M}\sum_{B>A}^{M} \frac{Z_A Z_B}{|\boldsymbol{R}_A - \boldsymbol{R}_B|} \tag{2.5}$$

Ψ granting $\delta E[\Psi] = 0$ is searched as the ground state wavefunction. Furthermore, H is Hermitian, and different wavefunctions Ψ are ortogonal. Additionaly, Ψ can be normalized, resulting with:

$$\int |\Psi|^2 \, d\boldsymbol{r}_i \, d\boldsymbol{r}_j ... \, d\boldsymbol{r}_N = 1 \tag{2.6}$$

Thus, eigenvalue E, the ground state energy, can also be stated as

$$E = \int \Psi^* H \Psi \, d\boldsymbol{r}_i \, d\boldsymbol{r}_j ... \, d\boldsymbol{r}_N \tag{2.7}$$

Moreover, eigenvalues of Hermitian H are real, and Ψ can be chosen as pure real for non-periodic setup where H is also real, thus Ψ^* does not have to be explicitly stated. Finally, note that the wavefunction Ψ is antisymmetric [3], meaning that sign of Ψ changes if two electrons are swapped. This requirement will be automatically satisfied within the Slater determinant construction of Kohn-Sham formalism.

2.2 Kohn-Sham density functional theory

Thomas-Fermi model [3] is an early density based approach, which replaces electronic wavefunction with density in energy calculation. This transformation reflects to electrostatic interaction energies trivially, as they can be simply stated with integrals instead of summations. Moreover, kinetic energy expression simplifies as well because now it is approximated as a functional of density. Nevertheless, this model proved to be very simple and not practical for molecules. Density functional theory was developed to be a viable tool thanks to the efforts of Hohenberg and Kohn [33] who showed that ground state density is uniquely mapped to an external potential and thus the ground state wavefunction of the system is defined by the external potential. Furthermore, Levy constrained-search method [34] ensured that ground state density indeed minimizes E.

Electron density of the system at $\boldsymbol{r}_i$ can be defined through the wavefunction Ψ as

$$\rho(\mathbf{r}_i) = N \int |\Psi|^2 \, d\boldsymbol{r}_j ... \, d\boldsymbol{r}_N \tag{2.8}$$

Note that, in that case:

$$N = \int \rho(\mathbf{r}) d\mathbf{r} \tag{2.9}$$

Electronic energy E is then defined as a functional of electron density:

$$E[\rho] = T[\rho] + E_{ee}[\rho] + E_{ne}[\rho] \tag{2.10}$$

Following these observations, Kohn-Sham [35] introduced a non-interacting reference system for electrons, and argued that an exchange-correlation term, E_{xc}, including the errors in both kinetic energy and electron-electron interaction energy must be added to (2.10) for the reference system to properly indicate the energy:

$$E_{KS}[\rho] = T[\rho] + E_{ee}[\rho] + E_{ne}[\rho] + E_{xc}[\rho] \tag{2.11}$$

Different models have been proposed to express $E_{xc}[\rho]$. A particularly common choice is local density approximation (LDA) based on uniform electron gas [3]. To account for the nonuniform effect, a different model, generalized gradient

approximation (GGA) was proposed. Unlike LDA, GGA incorporates density gradient as well in calculation of $E_{KS}[\rho, \nabla\rho]$.

(2.11) is to be minimized variationally. Using the Lagrange multipliers method, the functional $\Omega[\rho]$ is described as

$$\Omega[\rho] = E_{KS}[\rho] + \sum_{i=1}^{N} \epsilon_i \int (1 - |\Psi_i|^2)\, d\boldsymbol{r} \tag{2.12}$$

which enforces the normalization constraint on Kohn-Sham orbitals Ψ_i.

Since density is expressed in terms of wavefunctions, $\Omega[\rho]$ can be expressed as $\Omega[\psi_i]$. To find the ground state, $\delta\Omega[\psi_i] = 0$ is searched, which results in the following canonical Kohn-Sham equations

$$\hat{h}\psi_i = \epsilon_i \psi_i \tag{2.13}$$

with $\hat{h}$ as the one electron Hamiltonian operator:

$$\hat{h} = -\frac{1}{2}\nabla^2 + \upsilon_{eff} \tag{2.14}$$

Here, υ_{eff} is a collection of potentials acting on the wavefunction:

$$\upsilon_{eff} = \frac{\delta E_{ee}[\rho]}{\delta\rho} + \frac{\delta E_{en}[\rho]}{\delta\rho} + \frac{\delta E_{xc}[\rho]}{\delta\rho} = \upsilon_H + \upsilon_{ext} + \upsilon_{xc} \tag{2.15}$$

Finally, electron density is

$$\rho(\boldsymbol{r}) = \sum_{i=1}^{N} |\psi_i(\boldsymbol{r})|^2 \tag{2.16}$$

Presently, a closed shell structure will be assumed with equal occupancy values for spin-up and spin-down electrons. Therefore, (2.16) is restated as

$$\rho(\boldsymbol{r}) = 2\sum_{i=1}^{N/2} |\psi_i(\boldsymbol{r})|^2 \tag{2.17}$$

Consequently, in this spin-balanced context, individual energies are stated as

$$\begin{gathered} T = 2\sum_{i=1}^{N/2}(-\frac{1}{2}\nabla_i^2)\ , \quad E_{ne} = \int \rho(\boldsymbol{r})\upsilon_{ext}(\boldsymbol{r})\, d\boldsymbol{r} \\ E_{ee} = \frac{1}{2}\int \rho(\boldsymbol{r})\upsilon_H(\boldsymbol{r})\, d\boldsymbol{r}\ , \quad E_{xc} = \int \rho(\boldsymbol{r})\epsilon_{xc}(\boldsymbol{r})\, d\boldsymbol{r} \end{gathered} \tag{2.18}$$

Resulting total energy of the system E_{tot} is expressed as

$$\begin{aligned} E_{tot} &= T[\rho] + E_{ee}[\rho] + E_{ne}[\rho] + E_{nn}[\rho] + E_{xc}[\rho] \\ &= 2\sum_{i=1}^{N/2}(-\frac{1}{2}\nabla_i^2) + \frac{1}{2}\int \rho(\boldsymbol{r})\upsilon_H(\boldsymbol{r})\,d\boldsymbol{r} + \int \rho(\boldsymbol{r})\upsilon_{ext}(\boldsymbol{r})\,d\boldsymbol{r} + E_{nn} + \int \rho(\boldsymbol{r})\epsilon_{xc}(\boldsymbol{r})\,d\boldsymbol{r} \end{aligned} \tag{2.19}$$

Details regarding the calculation of E_{nn} will be discussed later.

Note that the one-electron Kohn-Sham equation is solved within a self consistent field (SCF) scheme in the sense that $\rho(\boldsymbol{r})$ needs to be known to calculate the operator $\hat{h}$ and thus $\psi_i(\boldsymbol{r})$, which in return will be used to calculate a novel $\rho(\boldsymbol{r})$. For this purpose, ψ_i's with the lowest ϵ_i's are interpreted to be contributing to the ground state wavefunctions at each iteration. Anderson mixing method is applied for $\rho(\boldsymbol{r})$ (and $\nabla\rho(\boldsymbol{r})$ in GGA) in calculation of $\hat{h}$ instead of using the exact $\rho(\boldsymbol{r})$ obtained through (2.17) [10]. SCF iterations are started with a suitable initial $\rho(\boldsymbol{r})$ guess. Convergence of both energy and l^2 norm of density are checked to stop SCF iterations.

2.3 Electrostatic problem

Total electrostatic potential, υ_C is defined as the sum of the Hartree potential υ_H and the external potential υ_{ext}, $\upsilon_C = \upsilon_H + \upsilon_{ext}$. υ_{ext}, υ_H and υ_C can be determined from nuclear and electronic charge distributions respectively by solving the following Poisson equations

$$-\frac{1}{4\pi}\nabla^2\upsilon_{ext}(\boldsymbol{r}) = b(\boldsymbol{r})\ , \quad -\frac{1}{4\pi}\nabla^2\upsilon_H(\boldsymbol{r}) = \rho(\boldsymbol{r})\ , \quad -\frac{1}{4\pi}\nabla^2\upsilon_C(\boldsymbol{r}) = b(\boldsymbol{r}) + \rho(\boldsymbol{r}) \tag{2.20}$$

where $b(\boldsymbol{r})$ denotes the nuclear charge distribution, and it is the sum of all individual nuclear charges:

$$b(\boldsymbol{r}) = \sum_{A=1}^{M} b_A(\boldsymbol{r}) \tag{2.21}$$

Definition of $b_A(\boldsymbol{r})$ is subject to the problem setting. In all-electron calculations, where nuclear charges are treated as point charges, $b_A(\boldsymbol{r})$ is constructed using

Dirac-delta function as

$$b_A(\boldsymbol{r}) = -Z_A\delta(\boldsymbol{r} - \boldsymbol{R}_A) \tag{2.22}$$

Equations (2.20) are subject to Dirichlet boundary conditions with υ_H decaying to 0 and υ_{ext} totaling of individual υ_A's . Note that a Poisson equation similar to that of υ_{ext} must be solved to project each υ_A onto the numerical discretization individually.

In the pseudopotential formulation, which consists of two parts as local and nonlocal, definitions of both $\upsilon_A(\boldsymbol{r})$ and $b_A(\boldsymbol{r})$ are altered [36] and are no longer in point charge form. In the local formulation, $\upsilon_A(\boldsymbol{r})$ is defined as a spherically symmetric function that is centered at the nucleus and behaves similar to point-charge induced potential beyond a certain radius. Resulting $b_A(\boldsymbol{r})$ is then also a spherically symmetric function concentrated in the vicinity of nucleus. Note that in the pseudopotential formulation Z_A is no longer the charge of the nucleus, but instead it is the charge of the ion. Nucleus-nucles interaction energy E_{nn} then can be expressed in a uniformed expression for all-electron and pseudopotential settings using $b(\boldsymbol{r})$ and $\upsilon_{ext}(\boldsymbol{r})$ in the following way:

$$E_{nn} = \frac{1}{2}\int b(\boldsymbol{r})\upsilon_{ext}(\boldsymbol{r})\,d\boldsymbol{r} - \frac{1}{2}\sum_{A=1}^{M}\int b_A(\boldsymbol{r})\upsilon_A(\boldsymbol{r})\,d\boldsymbol{r} \tag{2.23}$$

Note that the first term expresses the interaction of a nuclear charge with the total nuclear potential including the nucleus's own induced potential. Therefore, a self-interaction term is defined and subtracted as expressed by the second term. For pseudopotential calculations, classic form of E_{nn} expressed in (2.5) will also be used due to its compliance with reference calculations. This remark will be elaborated upon later.

Nonlocal pseudopotential formulation inherently can be handled separately. It does not contribute to the Poisson equation, but instead it constitutes its own energy functional E_{NL} via the nonlocal potential υ_{NL} as

$$E_{NL} = 2\sum_{i}^{N/2}\int \psi_i(\boldsymbol{r})\upsilon_{NL}(\boldsymbol{r},\boldsymbol{r'})\psi_i(\boldsymbol{r'})\,d\boldsymbol{r}\,d\boldsymbol{r'} \tag{2.24}$$

Therefore, nonlocal pseudopotential instead contributes to one electron Hamiltonian, which can be redefined as

$$\hat{h} = -\frac{1}{2}\nabla^2 + \upsilon_{eff} + \upsilon_{NL} \tag{2.25}$$

Note that in psedupotential formulation, Kohn-Sham equation is associated only with the valance electrons. In other words, N represents the number of valance electrons of the atom.

Similar to the local case, nonlocal potential [37] is a sum of ionic potentials. Using a separable form, the nonlocal pseudopotential for an ion is defined as

$$\begin{aligned} \Lambda_A &= \sum_{l=0}^{l_A} \Lambda_A^l(\boldsymbol{r}, \boldsymbol{r'}) \\ \Lambda_A^l(\boldsymbol{r}, \boldsymbol{r'}) &= \sum_{m=-l}^{l} \sum_{a=1}^{3} \sum_{b=1}^{3} Y_{lm}(\boldsymbol{r}) Y_{lm}(\boldsymbol{r'}) p_a^l(\boldsymbol{r}) p_b^l(\boldsymbol{r'}) h_{ab}^l \end{aligned} \tag{2.26}$$

where l and m denote the angular and magnetic quantum numbers respectively. Y_{lm} are the spherical harmonics, whereas p_a^l are called projectors. Along with parameters used to define local formulation, p_a^l and h_{ab}^l are ion-specific. Throughout this work, norm-conversing pseudopotentials are employed [37].

2.4 Revisiting the energy equation

Equation (2.19) currently lacks the nonlocal pseudopotential energy term, therefore it may be modified to include this term by addition of (2.24). υ_{NL} along with other potentials have already been used in calculation of orbital energies ϵ_i. Therefore, ϵ_i values which are already being calculated upon the solution of one-electron Kohn-Sham equation can be used to calculate kinetic energy in the following way:

$$T = 2\sum_{i}^{N/2} \epsilon_i - \int \rho(\boldsymbol{r}) \upsilon_{eff}(\boldsymbol{r})\, d\boldsymbol{r} - E_{NL} \tag{2.27}$$

Note that in this representation, nonlocal pseudopotential energy is inherently included in the term $2\sum_i^{N/2} \epsilon_i$. Kinetic energy expression above assumes close-shell structure with integer occupation numbers for each ϵ_i, either 0 or 1. Integer

occupancy constraint can be avoided through the use of fractional occupation numbers, leading to open-shell approximation. Fermi-Dirac smearing [11] is applied for this purpose, allowing the occupation number to be set as any number between 0 and 1. Thus, density, nonlocal energy and kinetic energy are restated as

$$\begin{gathered}\rho(\boldsymbol{r}) = 2\sum_{i=1}^{N/2} f_i|\psi_i(\boldsymbol{r})|^2, \quad E_{NL} = 2\sum_{i}^{N/2} f_i \int \psi_i(\boldsymbol{r})\upsilon_{NL}(\boldsymbol{r},\boldsymbol{r'})\psi_i(\boldsymbol{r'})\,d\boldsymbol{r}\,d\boldsymbol{r'}, \\ T = 2\sum_{i}^{N/2} f_i\epsilon_i - \int \rho(\boldsymbol{r})\upsilon_{eff}(\boldsymbol{r})\,d\boldsymbol{r} - E_{NL}\end{gathered} \tag{2.28}$$

Moreover, $\bar{\rho} = \rho + \rho_c$ in the context of NLCC where ρ_c is a sum of spherically symmetric core density contribution from each ion, and $\upsilon_{xc} = \tilde{\upsilon}_{xc} + \boldsymbol{\omega}_{xc}.\nabla$ in the context of GGA with $\boldsymbol{\omega}_{xc} = \{2\bar{\rho}\frac{\partial\epsilon_{xc}}{\partial\bar{\sigma}}\nabla\bar{\rho}\}$ where $\bar{\sigma} = |\nabla\rho_c|^2$. $\bar{\rho}$ and υ_{xc} will be used as generalized expressions that have disappearing terms ρ_c in the absence of NLCC effects as well as $\boldsymbol{\omega}_{xc}$ when LDA assumption is preferred. By updating the kinetic energy expression and substituting (2.23) for E_{nn}, total energy expression are restated as

$$\begin{aligned}E_{tot} =& 2\sum_{i}^{N/2} f_i\epsilon_i - \int \rho(\boldsymbol{r})\upsilon_{eff}(\boldsymbol{r})\,d\boldsymbol{r} + \frac{1}{2}\int \rho(\boldsymbol{r})\upsilon_H(\boldsymbol{r})\,d\boldsymbol{r} \; + \int \rho(\boldsymbol{r})\upsilon_{ext}(\boldsymbol{r})\,d\boldsymbol{r} \\ &+ \frac{1}{2}\int b(\boldsymbol{r})\upsilon_{ext}(\boldsymbol{r})\,d\boldsymbol{r} - \frac{1}{2}\sum_{A=1}^{M}\int b_A(\boldsymbol{r})\upsilon_A(\boldsymbol{r})\,d\boldsymbol{r} + \int \bar{\rho}(\boldsymbol{r})\epsilon_{xc}(\boldsymbol{r})\,d\boldsymbol{r}\end{aligned} \tag{2.29}$$

Finally, entropy [3] of the system can also be defined as

$$S = -2k\sum_{i}^{N/2}[f_i\ln(f_i) + (1-f_i)\ln(1-f_i)] \tag{2.30}$$

where k is the Boltzmann constant. Entropy will not be added to the energy expression, although its effect on force calculations will be discussed later.

2.5 FEM formulation

Kohn-Sham and Poisson equations are to be solved using the finite element method. Finite element method operates on a so-called weak-form [38], relaxing some of the conditions such as differentiability that the original equation is subject to. First, the Kohn-Sham equation is considered. To transform the equation to its weak form, the equation is first multiplied by a trial function φ that is assumed to decay at boundaries, and then the equations are integrated over the entire volume. Note that for simplicity, dependencies on $\boldsymbol{r}$ and differentials $d\boldsymbol{r}$ are not explicitly expressed. Integrals denoted by B are evaluated at the boundaries, otherwise integrations are evaluated over the whole volume. The weak form can be constructed through the following steps:

$$\int \varphi \hat{h} \psi_i = \int \varphi \epsilon_i \psi_i \tag{2.31}$$

$$\int \varphi (-\frac{1}{2}\nabla^2 + \upsilon_C + \upsilon_{xc} + \upsilon_{NL}) \psi_i = \int \varphi \epsilon_i \psi_i \tag{2.32}$$

$$\int \varphi (-\frac{1}{2}\nabla^2 + \upsilon_C + \tilde{\upsilon}_{xc} + \upsilon_{NL} + \boldsymbol{\omega}.\nabla) \psi_i = \int \varphi \epsilon_i \psi_i \tag{2.33}$$

Using the relation $a\nabla^2 b = \nabla.(a\nabla b) - \nabla a.\nabla b$ where both a and b are scalar and distributing each term, one obtains:

$$\int \Big(\nabla.(-\varphi\frac{1}{2}\nabla\psi_i) + \nabla\varphi.\frac{1}{2}\nabla\psi_i + \varphi\upsilon_c\psi_i + \varphi\tilde{\upsilon}_{xc}\psi_i + \varphi\upsilon_{NL}\psi_i + \nabla(\varphi\psi_i).\boldsymbol{\omega} - \nabla.(\varphi\boldsymbol{\omega}\psi_i) \Big) = \int \varphi\epsilon_i\psi_i \tag{2.34}$$

Using the gradient theorem, first and last terms on the left hand side can be described as a boundary integral instead of a volume integral:

$$\int \Big(\nabla\varphi.\frac{1}{2}\nabla\psi_i + \varphi\upsilon_C\psi_i + \varphi\tilde{\upsilon}_{xc}\psi_i + \varphi\upsilon_{NL}\psi_i + \nabla(\varphi\psi_i).\boldsymbol{\omega} \Big) + \int_B \Big(-\varphi\frac{1}{2}\nabla\psi_i + \varphi\boldsymbol{\omega}\psi_i \Big) = \int \varphi\epsilon_i\psi_i \tag{2.35}$$

Requiring $\varphi = 0$ at the boundary, the boundary integral cancels out and the following equation is obtained:

$$\int \Big(\nabla\varphi.\frac{1}{2}\nabla\psi_i + \varphi\upsilon_C\psi_i + \varphi\tilde{\upsilon}_{xc}\psi_i + \varphi\upsilon_{NL}\psi_i + \psi_i\nabla\varphi.\boldsymbol{\omega} + \varphi\nabla\psi_i.\boldsymbol{\omega} \Big) = \int \varphi\epsilon_i\psi_i \tag{2.36}$$

Inserting basis functions N_I for ψ_i and φ, discrete form of the Kohn-Sham equation is stated as $[H]\{\psi_i\} = \epsilon_i[M]\{\psi_i\}$ where

$$H_{IJ} = \int \nabla N_I . \frac{1}{2} \nabla N_J + \int N_I \upsilon_C N_J + \int N_I \tilde{\upsilon}_{xc} N_J + \int N_I \upsilon_{NL} N_J + \int N_J \nabla N_I . \boldsymbol{\omega} + \int N_I \nabla N_J . \boldsymbol{\omega} \tag{2.37}$$

$$M_{IJ} = \int N_I N_J \tag{2.38}$$

With real basis functions, matrices $[H]$ and $[M]$ are real. Moreover, they are sparse and symmetric due to the local support of the basis functions. Resulting discrete eigenvalue problem is then solved using Chebyshev-filtered subspace iteration method [39], upon adapting it to the generalized setting described above.

Poisson equation, which features far less terms, also needs to be transformed into the weak form. In a similar fashion, the equation is first multiplied by a trial function φ, and then integrated over the volume:

$$-\frac{1}{4\pi} \int \varphi \nabla^2 \upsilon_C = \int \varphi(\rho + b) \tag{2.39}$$

Using the relation $a\nabla^2 b = \nabla.(a\nabla b) - \nabla a.\nabla b$ and distributing each term, one obtains:

$$-\frac{1}{4\pi} \int \nabla.(\varphi \nabla \upsilon_C) + \frac{1}{4\pi} \int \nabla\varphi.\nabla\upsilon_C = \int \varphi(\rho + b) \tag{2.40}$$

First term on the left hand side can be stated as a boundary integral by using gradient theorem:

$$-\frac{1}{4\pi} \int_B \varphi \nabla \upsilon_C + \frac{1}{4\pi} \int \nabla\varphi.\nabla\upsilon_C = \int \varphi(\rho + b) \tag{2.41}$$

Since $\varphi = 0$, at the boundary, boundary integral cancels out and the following equation is obtained:

$$\frac{1}{4\pi} \int \nabla\varphi.\nabla\upsilon_C = \int \varphi(\rho + b) \tag{2.42}$$

φ and υ_C are expressed using basis functions N_I, resulting in the equation $[L]\{\upsilon_C\}=\{\mathrm{c}\}$ where

$$L_{IJ} = \frac{1}{4\pi} \int \nabla N_I . \nabla N_J \tag{2.43}$$

$$c_I = \int N_I(\rho + b) \tag{2.44}$$

2.6 Mesh construction

In the nonperiodic setting of this work, the boundary conditions require a geometry that is large enough to represent vacuum, where the wavefunctions are required to decay to zero at the boundaries. A sphere with an adaptable radius is constructed as the problem domain by using seven neighboring subdomains. Each subdomain, called a *patch* by convention, is constructed using NURBS basis functions [40]. Also used in CAD, NURBS basis functions allow exact, or nearly exact, construction of a desired geometry with a minimal number of degrees of freedom. The classical finite element method employing Lagrange basis functions is already isoparametric in nature, meaning that problem geometry can be expressed upon obtaining the solution field. However, the domain description must be updated upon mesh refinement. Using NURBS basis functions in construction of the mesh additionally transforms the analysis approach to what is called isogeometric [41], where problem geometry is set before obtaining the solution field and needs no further update.

Seven patches consist of one core patch, where atoms are placed and is denser in terms of elements, and six outer patches adjacent to the core patch. Element sizes in outer patches are gradually increased towards the boundary to resolve the vacuum. Shape of the patches are determined by control points, connection of which results in a control mesh resembling the final patch geometry. Control points are the degrees of freedom for a NURBS mesh. Setting the control points the same at patch boundaries for adjacent patches satisfies continuity between the patches. Each patch is further divided into elements by parametric points called knots, which are also used in calculation of basis functions. Note that NURBS basis functions of degree p are C^{p-1} continuous along knots, meaning that they are $p-1$ times differentiable, however their continuity can be decreased to any level from C^{p-2} to C^0 by manipulation of knots. Also, patches are constructed as being C^0 continuous at boundaries. If Lagrange basis functions are to be used in solution space, same procedure is followed in mesh construction, but unique knots are interpreted as degrees of freedom since they decide the element boundaries. These elements can then be combined with adjacent elements to

form new elements based on the desired degree p of Lagrange basis functions. The resulting discretization is interpolary, where NURBS are not. On the other hand, continuity across elements is always C^0 irrespective of degree p. Fig. 2.1 displays a sample two dimensional mesh for Lagrange and NURBS discretizations. Red dots represent the degrees of freedom of each mesh. Note that in Lagrange mesh degrees of freedom are exactly on the mesh geometry boundary, whereas NURBS mesh does not exhibit this interpolary behavior. Core patches colored by blue consist of two four radial elements for both meshes. Number of elements located radially along a Cartesian axis in the core patch will be denoted by e_o.

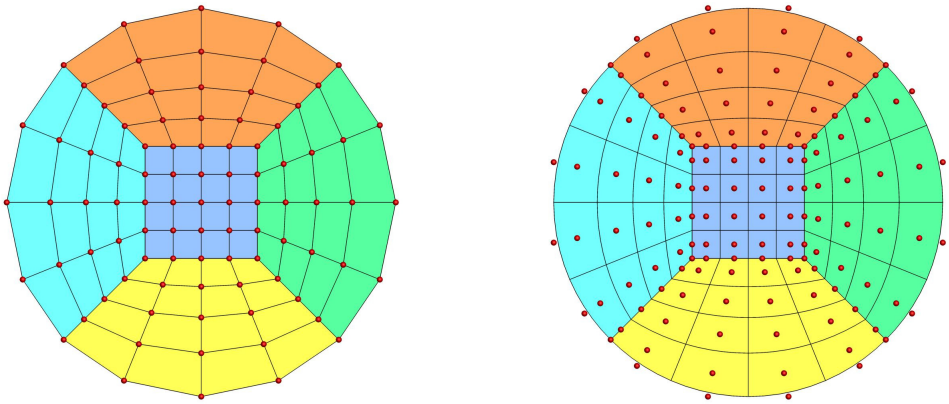

(a) 1^{st} order Lagrange mesh (b) 2^{nd} order NURBS mesh

Figure 2.1: Sample Lagrange and NURBS meshes

Furthermore, for all-electron calculations, mesh, and thus the basis functions, must be suitable to reflect a cusp behavior since nuclear charges are defined as point charges using Dirac functions. This can simply be achieved within the NURBS discretization by reducing continuity level to C^0 at the nuclear position through knot manipulation. For Lagrange discretizations, atoms can be placed at element boundaries where C^0 continuity naturally occurs.

Next, variationally consistent force expressions required to conduct geometry

optimization will be discussed.

Chapter 3

Derivation of force equations

Force expressions are obtained using Hellman-Feynman theorem, [12], which suggests that atomic forces are in fact simply the electrostatic interaction forces. Force on atom/ion A can be evaluated as the negative derivative of energy expression with respect to the atomic position:

$$\begin{aligned}
\boldsymbol{F}_A = -\frac{\partial E[\Psi]}{\partial \boldsymbol{R}_A} &= -\frac{\partial}{\partial \boldsymbol{R}_A}\int \Psi H \Psi \\
&= -\int \Psi \frac{\partial H}{\partial \boldsymbol{R}_A}\Psi - \int \frac{\partial \Psi}{\partial \boldsymbol{R}_A} H\Psi - \int \Psi H \frac{\partial \Psi}{\partial \boldsymbol{R}_A} \\
&= -\int \Psi \frac{\partial H}{\partial \boldsymbol{R}_A}\Psi - \int E[\Psi]\frac{\partial \Psi}{\partial \boldsymbol{R}_A} - \int E[\Psi]\frac{\partial \Psi}{\partial \boldsymbol{R}_A} \\
&= -\int \Psi \frac{\partial H}{\partial \boldsymbol{R}_A}\Psi - E[\Psi]\frac{\partial}{\partial \boldsymbol{R}_A}\int \Psi\Psi \\
&= -\int \Psi \frac{\partial H}{\partial \boldsymbol{R}_A}\Psi
\end{aligned} \tag{3.1}$$

Note that this derivation assumes basis functions are either not dependent on atomic positions or do form a complete basis set. Lack of these conditions results in an additional force term called Pulay force [13]. No Pulay forces are expected in current implementation due to the use of a fixed mesh. Result published in Hellman's original work is stated at (3.2). As it turns out, this result is only valid for all-electron case where υ_C is considered as purely discrete.

$$\boldsymbol{F}_A = (Z_A \nabla \upsilon_C - Z_A \nabla \upsilon_A \,)|_{\boldsymbol{R}_A} \tag{3.2}$$

Referring back to first line of (3.1), atomic forces can simply be calculated as the negative derivative of energy expression with respect to atomic positions. Energy expression in its expanded form is restated in (3.3), however note that the partial occupancies are omitted. Calculation of the derivative of occupancy numbers is rather tedious, and their effect on force calculations will be investigated later through examples. Hence, the energy equation is

$$\begin{aligned} E_{tot} =& 2\sum_{i}^{N/2} \epsilon_i - \int \rho \upsilon_{eff} + \frac{1}{2}\int \rho \upsilon_H + \int \rho \upsilon_{ext} \\ &+ \frac{1}{2}\int b\upsilon_{ext} - \frac{1}{2}\sum_{A=1}^{M}\int b_A \upsilon_A + \int \bar{\rho}\epsilon_{xc} \end{aligned} \tag{3.3}$$

For simplicity, let $(.)'$ denote a perturbation:

$$\begin{aligned} E'_{tot} =& 2\sum_{i}^{N/2} \epsilon'_i - \int \rho' \upsilon_{eff} - \int \rho \upsilon'_{eff} + \frac{1}{2}\int \rho' \upsilon_H \\ &+ \frac{1}{2}\int \rho \upsilon'_H + \int \rho' \upsilon_{ext} + \int \rho \upsilon'_{ext} \\ &+ \frac{1}{2}\int b' \upsilon_{ext} + \frac{1}{2}\int b\upsilon'_{ext} \\ &- \frac{1}{2}\sum_{A=1}^{M}\int b'_A \upsilon_A - \frac{1}{2}\sum_{A=1}^{M}\int b_A \upsilon'_A \\ &+ \int \bar{\rho}' \epsilon_{xc} + \int \bar{\rho}\epsilon'_{xc} \end{aligned} \tag{3.4}$$

Note that if occupation numbers were not omitted, first term of the force expression would be

$$2\sum_{i}^{N/2} f'_i \epsilon_i + 2\sum_{i}^{N/2} f_i \epsilon'_i \tag{3.5}$$

Additionally, variation of the entropy contribution would have to be considered. Implications of these additional term will be discussed later. Continuing with the derivation, first the term $2\sum_i^{N/2} \epsilon'_i$ is analyzed using the one-electron Kohn-Sham

equation:

$$\begin{aligned}
(h\psi_i)' &= (\epsilon_i\psi_i)' \\
h'\psi_i + h\psi_i' &= \epsilon_i'\psi_i + \epsilon_i\psi_i' \\
\psi_i h'\psi_i + \psi_i h\psi_i' &= \psi_i\epsilon_i'\psi_i + \psi_i\epsilon_i\psi_i' \\
\int \psi_i h'\psi_i + \int \psi_i h\psi_i' &= \int \psi_i\epsilon_i'\psi_i + \int \psi_i\epsilon_i\psi_i' \\
\int \psi_i h'\psi_i + \int \psi_i\epsilon\psi_i' &= \int \psi_i\epsilon_i'\psi_i + \int \psi_i\epsilon_i\psi_i' \\
\int \psi_i h'\psi_i &= \int \psi_i\epsilon_i'\psi_i \\
\int \psi_i(\upsilon_{eff}' + \upsilon_{NL}')\psi_i &= \epsilon_i'
\end{aligned} \tag{3.6}$$

Later, individual ϵ_i''s are summed up as

$$\begin{aligned}
2\sum_i^{N/2}\epsilon_i' &= \int \upsilon_{eff}'\ 2\sum_i^{N/2}|\psi_i|^2 + 2\sum_i^{N/2}\int \psi_i\upsilon_{NL}'\psi_i \\
&= \int \rho\upsilon_{eff}' + 2\sum_i^{N/2}\int \psi_i\upsilon_{NL}'\psi_i
\end{aligned} \tag{3.7}$$

The derivation is continued by working on terms of the third row of (3.4) through a similar procedure as in weak formulation transformation in FEM:

$$\begin{aligned}
-\nabla^2\upsilon_{ext} &= 4\pi b \\
\int -\varphi\nabla^2\upsilon_{ext} &= \int 4\pi\varphi b \\
\int \nabla\upsilon_{ext}.\nabla\varphi - \int_B \varphi\nabla\upsilon_{ext}.\boldsymbol{n} &= 4\pi\int \varphi b
\end{aligned} \tag{3.8}$$

Inserting $\varphi = \upsilon_{ext}'$; $\int \nabla\upsilon_{ext}\nabla\upsilon_{ext}' - \int_B \upsilon_{ext}'\nabla\upsilon_{ext}.\boldsymbol{n} = 4\pi\int \upsilon_{ext}' b$. Similarly;

$$\begin{aligned}
-\nabla^2\upsilon_{ext}' &= 4\pi b' \\
\int -\varphi\nabla^2\upsilon_{ext}' &= \int 4\pi\varphi b' \\
\int \nabla\upsilon_{ext}'\nabla\varphi - \int_B \varphi\nabla\upsilon_{ext}'.\boldsymbol{n} &= 4\pi\int \varphi b'
\end{aligned} \tag{3.9}$$

Inserting $\varphi = \upsilon_{ext}$; $\int \nabla\upsilon_{ext}\nabla\upsilon_{ext}' - \int_B \nabla\upsilon_{ext}'\upsilon_{ext}.\boldsymbol{n} = 4\pi\int \upsilon_{ext} b'$. Provided that the domain is large enough for the boundary terms to vanish, one therefore finds

$\int \upsilon'_{ext} b = \int \upsilon_{ext} b'$. In a similar fashion, one can show that $\int \upsilon'_H \rho = \int \upsilon_H \rho'$ and $\int \upsilon'_A b_A = \int \upsilon_A b'_A$. While combining equal terms, the charge-perturbed expressions will be preferred.

Finally, last two terms in (3.4), relating to exchange-correlation are considered:

$$\begin{aligned}
\int \bar{\rho}' \epsilon_{xc} + \int \bar{\rho} \epsilon'_{xc} &= \int \bar{\rho}' \epsilon_{xc} + \int \bar{\rho} \frac{\delta \epsilon_{xc}}{\delta \bar{\rho}} \bar{\rho}' \\
&= \int \bar{\rho}' \upsilon_{xc} \\
&= \int \rho' \upsilon_{xc} + \int \rho'_c \upsilon_{xc} \\
&= \int \rho' \upsilon_{xc} + \int \rho'_c \tilde{\upsilon}_{xc} + \int \nabla(\rho'_c) \boldsymbol{\omega}_{xc}
\end{aligned} \tag{3.10}$$

Using the results (3.6) to (3.10), E' is simplified as

$$\begin{aligned}
E'_{tot} = \quad & \int \rho \upsilon'_{eff} + 2 \int \psi(\boldsymbol{r}) \upsilon'_{NL} \psi \\
& - \int \rho \upsilon'_{eff} + \int \rho' (\upsilon_{ext} + \upsilon_H + \upsilon_{xc} - \upsilon_{eff}) \\
& + \int \rho \upsilon'_{ext} + \int b' \upsilon_{ext} \; - \sum_A \int b'_A \upsilon_A \\
& + \int \rho'_c \tilde{\upsilon}_{xc} + \int (\rho'_c)' \boldsymbol{\omega}_{xc} \\
= \quad & \int \rho \upsilon'_{ext} + \int b' \upsilon_{ext} \; - \sum_A \int b'_A \upsilon_A \\
& + 2 \sum_i^{N/2} \int \psi_i \upsilon'_{NL} \psi_i + \int \rho'_c \tilde{\upsilon}_{xc} + \int \nabla(\rho'_c) \boldsymbol{\omega}_{xc}
\end{aligned} \tag{3.11}$$

Note that regarding (3.11), in the absence of nonlocal pseudopotential and NLCC+GGA contributions, all terms on the second row vanish. Now, by choosing the perturbation to be associated with an atomic position $(.)' = -\frac{\partial}{\partial \boldsymbol{R}_A}(.) = \frac{\partial}{\partial \boldsymbol{r}}(.)|_{\boldsymbol{r}=\boldsymbol{R}_A}$, the final force expression is derived:

$$\begin{aligned}
\boldsymbol{F}_A = \quad & \int \rho \nabla \upsilon_A + \int \nabla b_A \upsilon_{ext} \; - \int \nabla b_A \upsilon_A \\
& + 2 \sum_i^{N/2} \int \psi_i \nabla \upsilon_{NL} \psi_i + \int \nabla \rho_c \tilde{\upsilon}_{xc} + \int \boldsymbol{P} \boldsymbol{\omega}_{xc}
\end{aligned} \tag{3.12}$$

Here, $\boldsymbol{P} = \nabla(\nabla\rho_c)$, first term represents the force on atom/ion A induced by electron density, the second term represents the force induced by nuclear charges, and third force term is the nuclear self-interaction force. First term on the second row is the force due to the nonlocal effects, while the remaining terms stem from GGA+NLCC assumption.

One must be careful with nuclear potential choices in force calculation. If nuclear energy E_{NN} is calculated using the discrete potentials obtained through the solution of nuclear Poisson equation, then force calculation must follow this choice. Of course, using exact potentials is the second choice. However, Kohn-Sham equation is always constructed using exact nuclear potentials, thus this argument does only apply to second and third term, and υ_A in the first term is always exact. If the definition of E_{nn} is changed to (2.5), then second and third terms are replaced by $\sum_{B=1}^{M,M\neq A} Z_A Z_B \frac{\boldsymbol{R}_A - \boldsymbol{R}_B}{|\boldsymbol{R}_A - \boldsymbol{R}_B|^3}$. Indeed, for pseudopotential calculations this will be the choice to represent nuclear-nuclear interactions because of its compliance with reference values generated via other quantum mechanics softwares.

One final remark is for all-electron calculations. It is useful to remind that b is point charge in nature and pseudopotential induced spherically symmetric υ_A does not exist. In that case, one can show that the term $\int \rho\upsilon'_{ext}$ can be replaced by $\int b'\upsilon_H$ within the finite element weak form provided that υ_{ext} is represented in discrete form similar to υ_H. Since b is represented by Delta dirac function, terms with b' are evaluted at $\boldsymbol{r} = \boldsymbol{R}_A$ as well and the overall force expression neglecting GGA+NLCC terms simplifies to

$$\begin{aligned} \boldsymbol{F}_A = \int b'_A\upsilon_H + \int b'_A\upsilon_{ext} - \int b'_A\upsilon_A &= \int b'_A\upsilon_C - \int b'_A\upsilon_A \\ &= (Z_A\nabla\upsilon_C - Z_A\nabla\upsilon_A\ )|_{\boldsymbol{R}_A} \end{aligned} \tag{3.13}$$

Hence, only in the all-electron setting under the stated conditions, the atomic forces are in the classical form (3.2) as previously stated.

Forces calculated using the derived force expressions will be called analytical forces for the rest of this work. Computational results for analytical forces will be introduced in the next chapter.

Chapter 4

Pseupotential force calculations

4.1 Single atom case

A single atom in a vacuum is expected to undergo zero force. Since there are no other atoms to interact with, the only possible nonzero force components results from density-ion interaction. Indeed, if the density distribution is resolved well enough upon satisfying a high density tolerance at SCF solution, a zero total force will be calculated as expected. However, this calculation is only valid for a single geometry configuration, where the single atom is placed at the center of the mesh. Placing the atom non-symmetric with respect to any Cartesian axis causes a nonzero force component in that respective axis. This observation can be explained by the egg-box effect [27], which indicates that energy of a molecule and the individual forces acting on the molecule's atoms undergo oscillations as the molecule is translated. To display this phenomenon, a lithium atom, initially placed at the center of the mesh, is translated by equal steps of [0, 0.03, 0.1] Bohr. Fig. 4.1-4.4 display the oscillations the atom undergo. It is observed that increasing the solution quality, either by increasing the basis function order or the element number, reduces the egg-box oscillations.

The terminology used to define calculation setups is briefly commented upon.

Characters N and L stand for NURBS and Lagrange, and are used to identify the type of the basis function used. First number next to a character is the order of the basis function. Finally, number followed by "-" is e_o. For instance, a solution labeled L3-12 is obtained using 3$^{\text{rd}}$ order Lagrange basis with a mesh containing 12 elements in x-direction in the core patch.

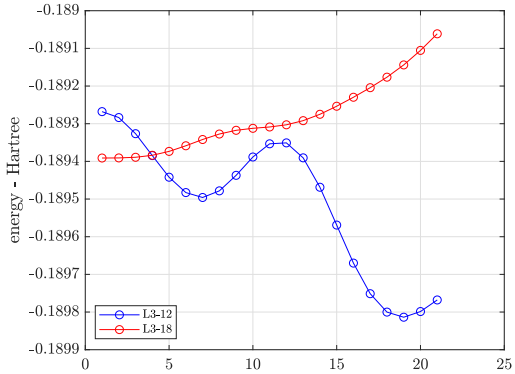

(a) lithium atom - energy

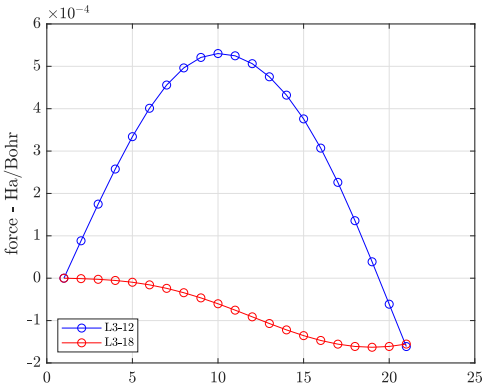

(b) lithium atom - y-force component

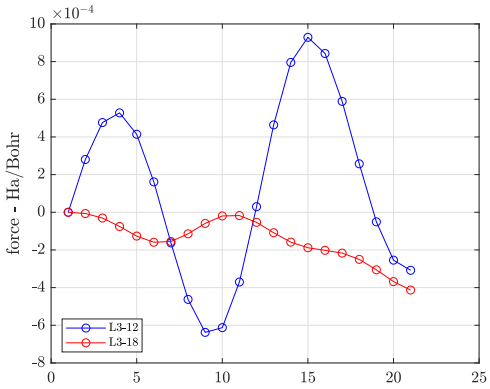

(c) lithium atom - z-force component

Figure 4.1: Effect of element number on egg-box effect for 3$^{\text{rd}}$ order Lagrange basis - each point is captured with a translation of [0, 0.03, 0.1] Bohr with respect to the previous point

Fig. 4.1 displays the effect of number of elements on the egg-box effect. Both the energy and force components display visibly greater oscillations in the setup with less elements. Also, egg-box effect is harder to observe in the direction where the atom is translated less. Note that since the atom is not translated along the x-direction, the system is still symmetric with respect to the x-axis and

an egg-box related force is not observed.

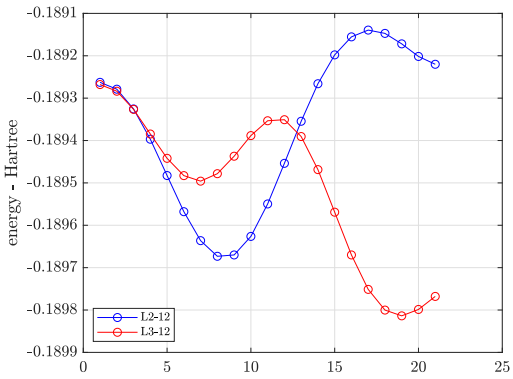

(a) lithium atom - energy

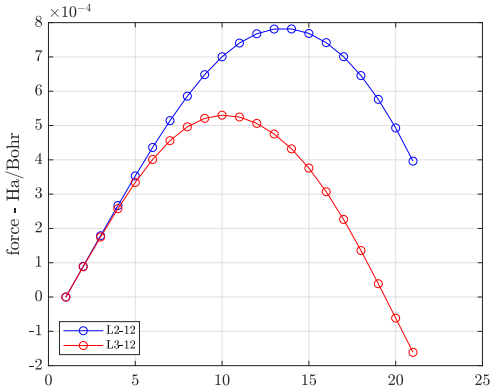

(b) lithium atom - y-force component

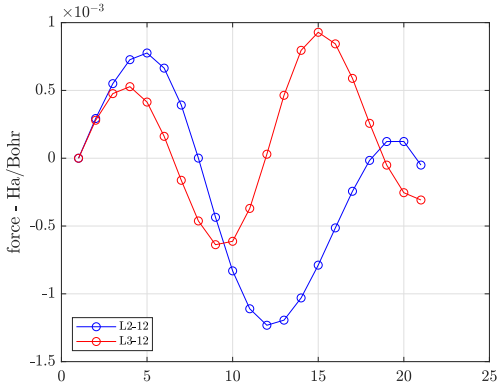

(c) lithium atom - z-force component

Figure 4.2: Effect of Lagrange basis function order on egg-box effect for fixed element number - each point is captured with a translation of [0, 0.03, 0.1] Bohr with respect to the previous point

Fig. 4.2 demonstrates the effect of order of Lagrange basis function on the egg-box effect. Order is increased from 2 to 3, while the number of elements is kept the same. For y and z force components, egg-box effect is greater for 2^{nd} order basis functions. Even though oscillation magnitudes in energies are significantly closer compared to the previous example, setup with 2^{nd} order basis functions still yields higher oscillations.

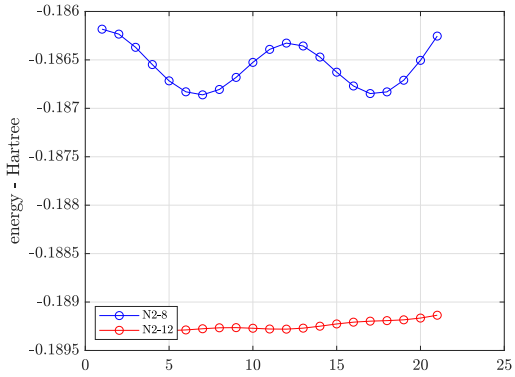

(a) lithium atom - energy

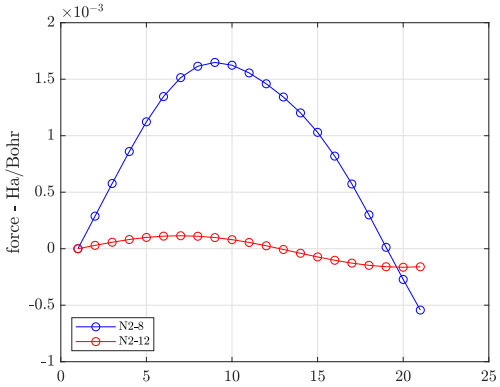

(b) lithium atom - y-force component

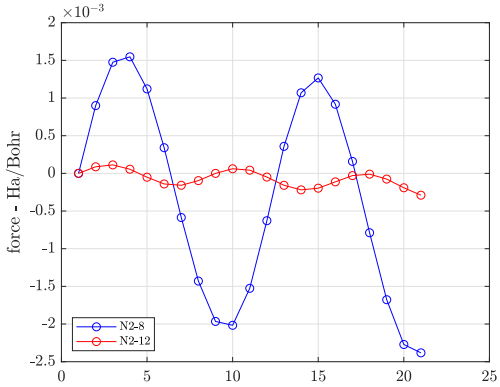

(c) lithium atom - z-force component

Figure 4.3: Effect of element number on egg-box effect for 2nd order NURBS basis - each point is captured with a translation of [0, 0.03, 0.1] Bohr with respect to the previous point

Fig. 4.3 and Fig 4.4 display similar results for NURBS basis functions. Increasing the solution quality either by increasing the basis function order or increasing the element number clearly reduces the egg-box effect. Although, it must be noted that N2-12 and N3-12 setup demonstrated extremely close oscillation behaviors in force components, which is an indication of an already very high quality in solution while resolving the density distribution.

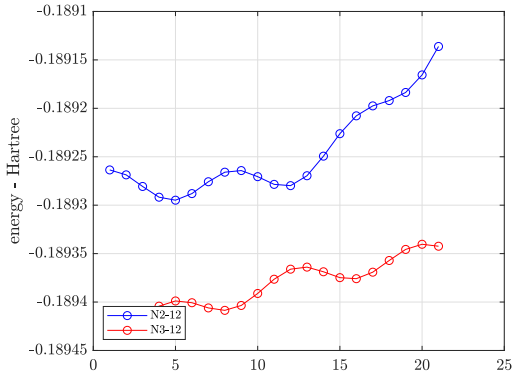

(a) lithium atom - energy

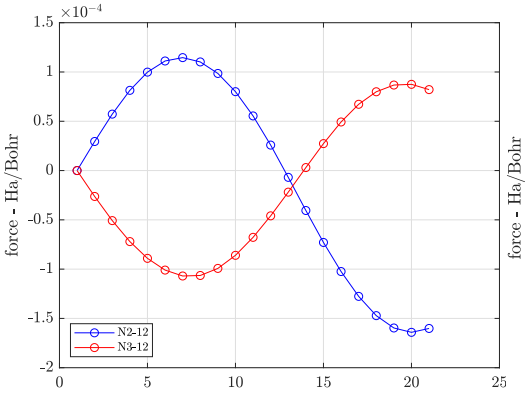

(b) lithium atom - y-force component

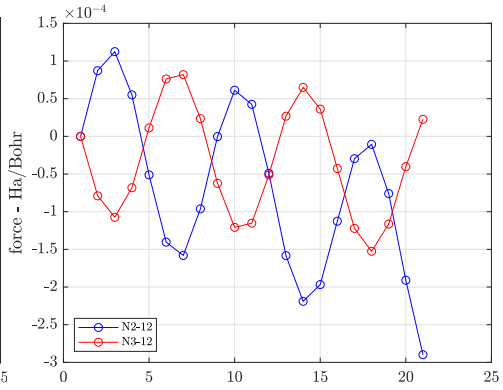

(c) lithium atom - z-force component

Figure 4.4: Effect of NURBS basis function order on egg-box effect for fixed element number - each point is captured with a translation of [0, 0.03, 0.1] Bohr with respect to the previous point

4.2 Two atom case

Unlike the single atom case, the nuclei in a molecule are expected to experience forces unless the molecule is in its ground state configuration. Therefore, a diatomic molecule of any bond length except the ground state bond length must display a force. Moreover, ideally forces on both atoms must be of equal magnitude and opposite direction. However, as in the case of the single atom, egg-box effect is still relevant when the molecule is not placed symmetrically in the mesh.

To demonstrate that egg-box effect is observed in molecules as well, an H_2 molecule with atoms initially placed at (-1.0,-0.5,0) and (0.7833,0.4,0.1) is translated by [0.01,0.03,0.1]. Results are displayed in Fig. 4.5 and Fig. 4.6 for Lagrange and NURBS basis respectively. For both figures, blue force represents the force on atom at (-1.0,-0.5,0), while the red data belongs to the second atom. Green lines represent the force magnitude that is expected for this setup if atoms were placed symmetrically in the mesh with no egg-box forces occurring. Forces on both atoms are observed to oscillate with similar periods. Also, note that magnitude of oscillations in forces are higher than that of energies. This observation is expected since energy perturbation scales with the square of density perturbation, whereas force perturbation scales directly with density perturbation.

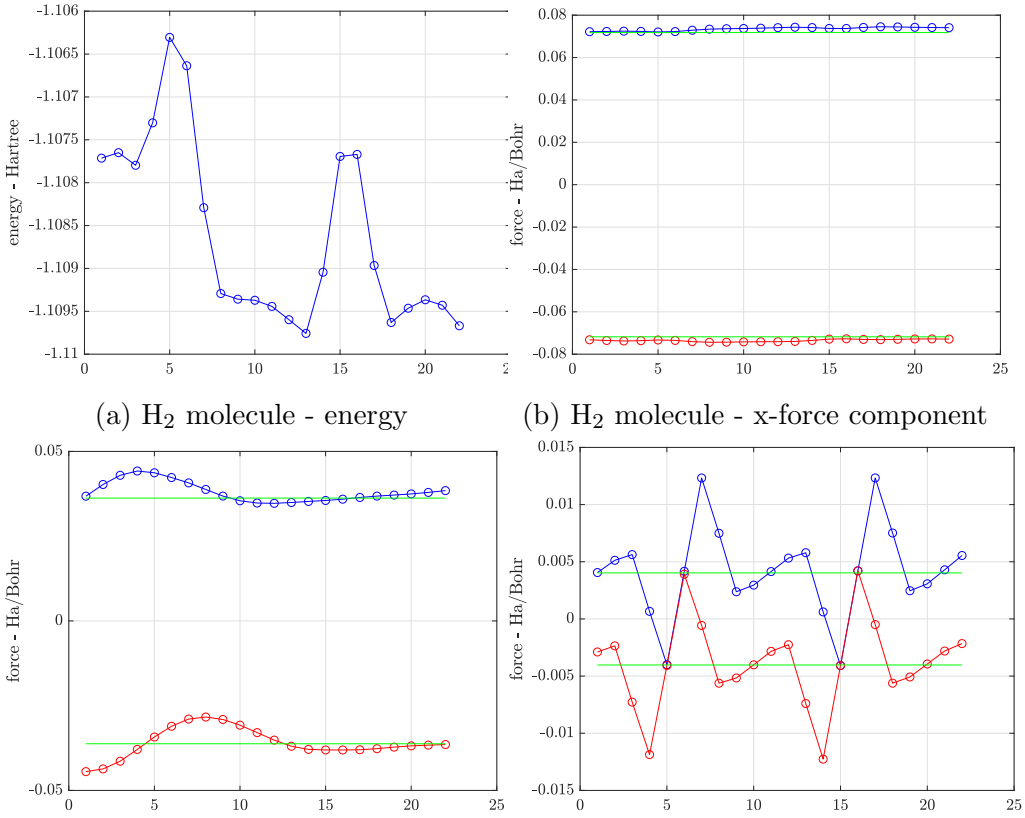

(a) H_2 molecule - energy

(b) H_2 molecule - x-force component

(c) H_2 molecule - y-force component

(d) H_2 molecule - z-force component

Figure 4.5: Egg-box effect in L3-18 using H_2 molecule - each point is captured with a translation of [0.01,0.03,0.1] Bohr with respect to the previous point

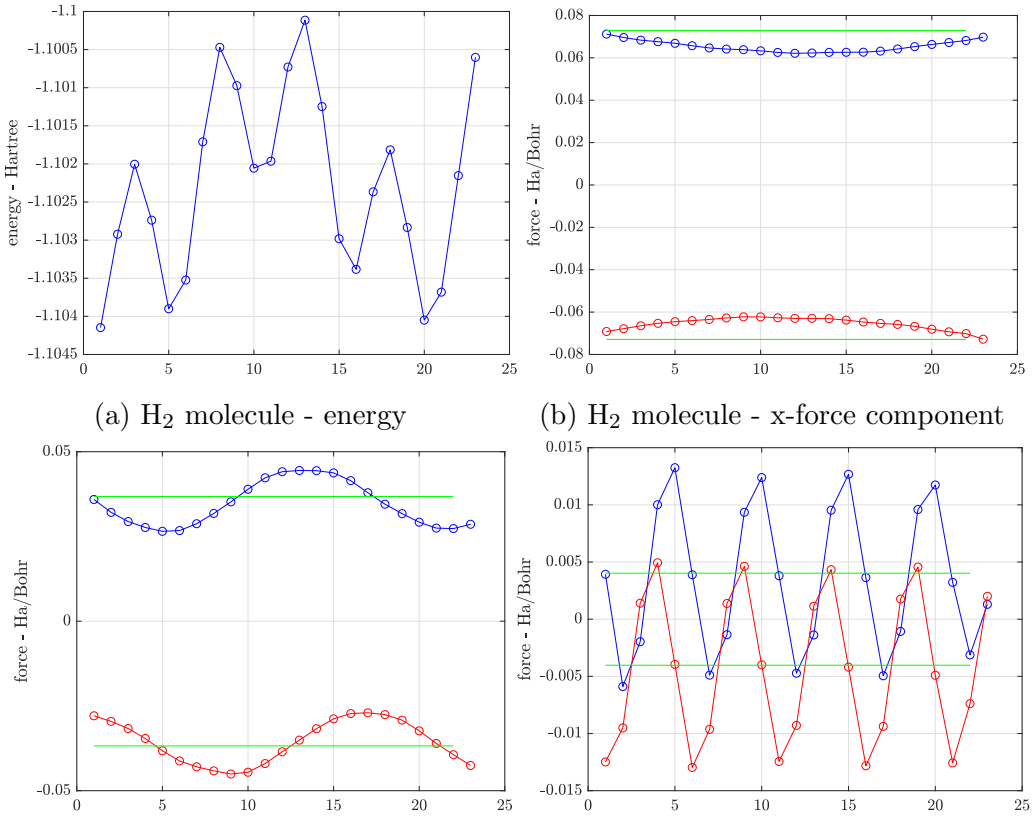

(a) H_2 molecule - energy

(b) H_2 molecule - x-force component

(c) H_2 molecule - y-force component

(d) H_2 molecule - z-force component

Figure 4.6: Egg-box effect in N3-12 using H_2 molecule - each point is captured with a translation of [0.01,0.03,0.1] Bohr with respect to the previous point

Furthermore, accuracy and variational consistency of the forces calculated can be checked using finite difference (FD) method [42]. One way to achieve this is to change the bond length as if creating an energy-length curve by perturbing both atoms with the same magnitude. Absolute value of the derivative of this curve must be equal to the magnitude of forces acting on the atom. A brief review of finite difference method with its application to the current problem is needed. Using second order central finite difference method where each atom is perturbed by Δ force on atom A is

$$F_A(\mathbf{R}) = \frac{E(\mathbf{R}+\Delta) - E(\mathbf{R}-\Delta)}{2\Delta} \tag{4.1}$$

with the leading error term $\frac{\Delta^2(E'''(\mathbf{R}+\Delta)-E'''(\mathbf{R}-\Delta))}{12}$. Since evaluating the third derivative of energy is not desired, a small perturbation amount must be selected for numerical safety. Trials showed that a perturbation amount of 10^{-4} or 10^{-5} is sufficiently small. Also, it must be noted that finite difference method can only produce a guess up one digit less than that of converged energy.

Even though energy convergence is sufficient to calculate the finite difference force, which itself is automatically variational because it is calculated using the energy, accuracy of the analytical force depends heavily on the density convergence. As density convergence tails energy convergence, stopping SCF iterations prematurely without setting a high density tolerance yields highly inaccurate results. Force convergence has been observed to tail density convergence by at most one less digit after the decimal point. Therefore, for instance if 10^{-5} accuracy is required in analytical force, density convergence tolerance must be set to 10^{-6}.

If the analytical forces are in compliance with FD forces, they are deemed to be 'variationally consistent', for they indeed are forces for that specific setup that yields variational energies. Note that FD method is impractical to use with large systems where numerous perturbations must be applied to calculate the force on each atom.

4.2.1 Local pseudopotential calculations

H_2 molecule is chosen to conduct local pseudopotential calculations, considering H, apart from He, is the only atom that does not have any nonlocal contribution in its pseudopotential formulation.

A preliminary example of force calculation is conducted on an N3-8 setup with LDA. Atoms are placed symmetrically in mesh, and both are perturbed to obtain the bond lengths indicated in Table 4.1. 2^{nd} FD force is then calculated using respective energies.

Bond length [Bohr]	Energy [Ha]	Analytical force [Ha/Bohr]	FD force [Ha/Bohr]	Difference [Ha/Bohr]
1.99999	-1.095273001293			
2.00000	-1.095271928999	0.1031785789	0.107229750	$4.1\text{x}10^{-3}$
2.00001	-1.095270856698			

Table 4.1: Force on H_2 molecule - N3-8

Even though chemical accuracy of forces [8] is only checked at the convergence of forces through refinement, chemical accuracy value 10^{-4} Hartree/Bohr will still be used as test parameter in coarse meshes. Analyzing Table 4.1, if the calculation was done at chemically accurate energy, resultant force difference would be much higher than desired chemical accuracy in force. Fortunately, force difference can be reduced to values well below of the chemical accuracy by increasing the integration accuracy. In the preliminary example, 4 integration points were used per element direction. By adding 2 more integration points, following result in Table 4.2 is obtained:

Bond length [Bohr]	Energy [Ha]	Analytical force [Ha/Bohr]	FD force [Ha/Bohr]	Difference [Ha/Bohr]
1.99999	-1.096667818703			
2.00000	-1.096666822344	0.099591519	0.09963599	$4.4\text{x}10^{-5}$
2.00001	-1.096665825983			

Table 4.2: Force on H_2 molecule with reduced integration error- N3-8

Chemical accuracy is therefore satisfied by reducing the integration error.

To test the limits of finite difference test, an N3-12 setup where the integration error is 10^{-10} Hartree in energy is constructed. Note that, energy and density convergence tolerances were kept small enough for the analytical and FD forces to be accurate to 10^{-12} precision.

Bond length [Bohr]	Energy [Ha]	Analytical force [Ha/Bohr]	FD force [Ha/Bohr]	Difference [Ha/Bohr]
1.99999	-1.08006073433003			
2.00000	-1.08005767945100	0.305488559949	0.305488559491	$1.5\text{x}10^{-10}$
2.00001	-1.08005462455884			

Table 4.3: Force on H_2 molecule with reduced integration error - N3-12

As can be seen from Table 4.3, force difference can be reduced to same magnitude of the integration error. Note that the N3-8 setup was incapable of accomplishing the desired integration accuracy, therefore an N3-12 setup was used for this example. Since $\Delta^2 = 10^{-10}$ as well, numerical accuracy of the second order finite difference method could be questioned as well. This issue is investigated at Appendix A, and for this particular example second order finite difference method is deduced to be at least 10^{-10} accurate.

Another parameter affecting the accuracy of forces calculated is the mesh size. Using the same setup (N3-8, with additional integration points) for Table 4.2, radius of the mesh is gradually increased. Results are shown in Table 4.4.

Mesh radius [Bohr]	Analytical force [Ha/Bohr]	FD force [Ha/Bohr]	Difference [Ha/Bohr]
20	0.0960986	0.0963205	0.0002219
30	0.0961416	0.0962898	0.0001482
100	0.0995915	0.0996360	0.0000445
150	0.0996068	0.0996364	0.0000296

Table 4.4: Effect of mesh radius on force - N3-8

A simple conclusion to draw so far is that accuracy of forces is greatly affected by the integration error and the mesh size. As these effects are reduced, the agreement between the analytical and FD forces increases.

Upon these observations, energy and force behavior for H_2 molecule around

equilibrium is presented in Fig. 4.7. Note that the setup used for this example (N3-16) has not achieved chemical accuracy in energy, therefore its equilibrium bond length does not reflect the true bond length for the molecule.

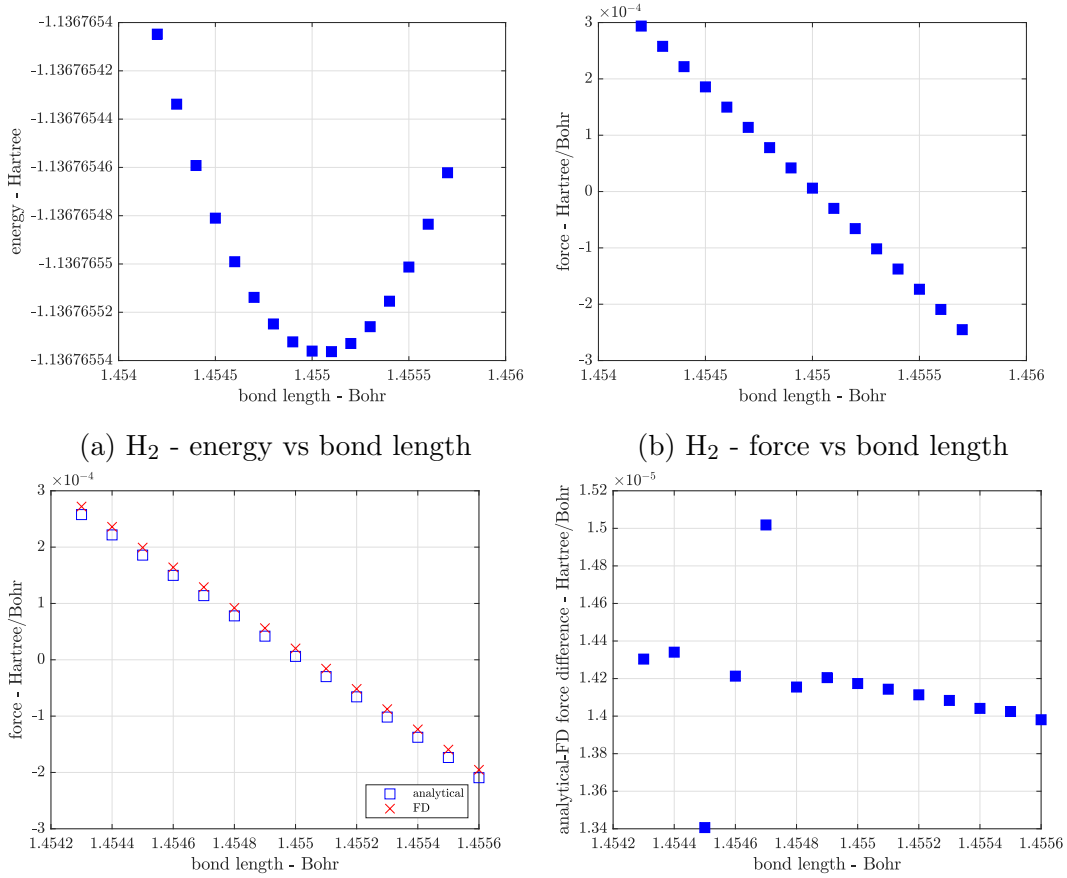

(a) H_2 - energy vs bond length

(b) H_2 - force vs bond length

(c) H_2 - force vs bond length

(d) H_2 - force difference vs bond length

Figure 4.7: Energy and force curves for H_2 around equilibrium - N3-16

Furthermore, analytical force must be consistent with FD force even when egg-box effect is relevant. Constructing the same setup for Table 4.1 by using 2 additional integration points. molecule is translated along the x-axis; first H atom is placed at (-0.5,0.0,0.), while the second one is placed at (1.5,0.0,0.0), thus keeping the 2.0 Bohr bond length previously used. Unlike the previous examples, only one atom, on which force is calculated, is perturbed. Results for both atoms are displayed in Table 4.5.

Coordinate [Bohr]	Analytical force [Ha]	FD force [Ha/Bohr]	Difference [Ha/Bohr]
(-0.5,0.0,0)	0.067242894305	0.067198398312044	$4.45\text{x}10^{-5}$
(1.5,0.0,0)	-0.076836809595	-0.076834329453875	$2.48\text{x}10^{-6}$

Table 4.5: Force on non-symmetric H_2 molecule - N3-8

As a remark, if both atoms were perturbed as previously, FD force matches half the difference of individual forces on the atoms because the analytical force is always compatible with only a single-atom perturbation.

Moreover, it is possible to fit a curve to bond length-energy graph, and use the derivative of this curve to describe the bond length-force relation. Same setup for Fig. 4.7 is used, however, bond length is perturbed significantly more to eliminate linearity in force in vicinity of equilibrium bond length. A cubic spline curve is evaluated as the fit for the energy curve, and its derivative is mapped to the bond length-force curve, as shown in Fig. 4.8.

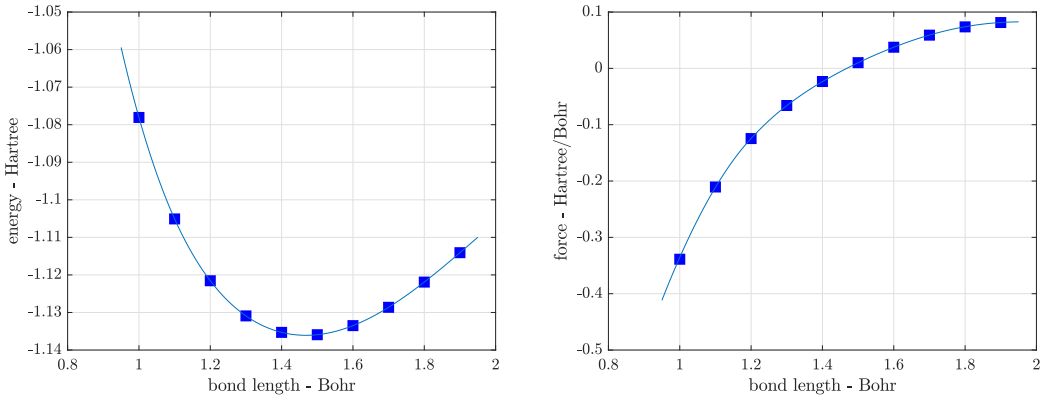

(a) H_2 - energy vs bond length (b) H_2 - force vs bond length

Figure 4.8: Energy and force curves for H_2 around equilibrium with fitting cubic spline interpolation. Derivative of energy curve is mapped to the force curve. - N3-16

Having established that analytical forces are variationally consistent, they also

need to be compared with reference values from the literature. For local LDA calculations, ABINIT [43] software is used to generate reference values. H_2 molecule with a bond length 2.0 Bohr is chosen as the example. ABINIT deduces that the magnitude of the force acting on each atom is 0.081990 Bohr/Hartree, where the reported value is to the given accuracy. Convergence of analytical forces upon mesh refinement is investigated as shown in Fig. 4.9 with the black bars indicating the chemical accuracy [8] border, 10^{-4} Ha/Bohr on each atom.

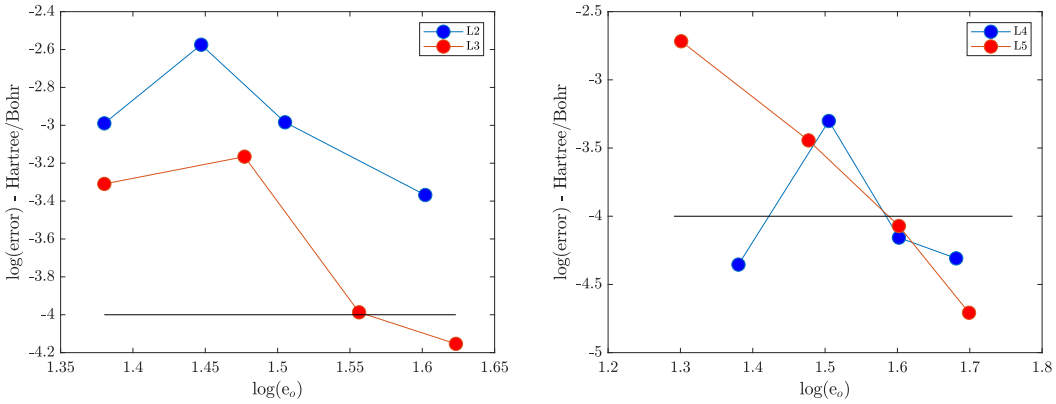

(a) H_2 - with L2 and L3 basis

(b) H_2 - with L4 and L5 basis

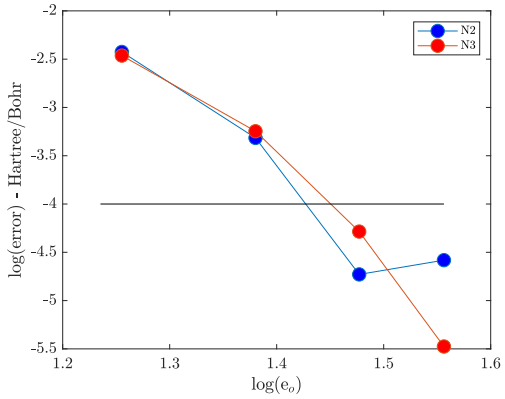

(c) H_2 - with N2 and N3 basis

Figure 4.9: Force convergence for H_2 upon mesh refinement

Although no systematic convergence is observed, due to the lack of a variational principle for the forces, forces calculated at most refined meshes tend to yield better results. Note that chemical accuracy was not reached with 2^{nd} order Lagrange basis due to slow convergence, which highlights the importance of using

higher-order elements.

4.2.2 Nonlocal pseudopotential calculations

F_2 molecule is chosen to conduct nonlocal pseudopotential calculations. Observations regarding the local calculations are expected to hold for nonlocal calculations as well, since nonlocal pseudopotential does not replace local pseudopotential, but it is rather an extra contribution. In the nonlocal pseudopotential case, GGA is used along with NLCC to demonstrate capability of force calculations with GGA+NLCC. As previously done, integration error is reduced to show the compliance of analytical force with FD force. An example calculation is presented in Table 4.6.

Bond length [Bohr]	Energy [Ha]	Analytical force [Ha/Bohr]	FD force [Ha/Bohr]	Difference [Ha/Bohr]
1.99999	-48.29583372936			
2.00000	-48.29584434774	1.06181347918	1.06181348477	$5.6\text{x}10^{-10}$
2.00001	-48.29585496563			

Table 4.6: Force on F_2 molecule - N3-16 with reduced integration error

Similar to H_2, energy and force behavior for F_2 molecule around the equilibrium is presented in Fig. 4.10 . Again, note that these results are not obtained at chemical accuracy.

Note that while deriving force equations, occupancy term f_i was omitted, however it is observed that change in orbital occupation affects the accuracy of FD force. SCF solution for F_2 molecule usually results in equal occupancy numbers upon small perturbation, therefore Be_2 molecule is chosen to demonstrate this effect. First, a case with bond length of 2.0 Bohr where this effect may not be relevant at a first glance is presented. With this setup, difference between the analytical and FD force is $7.33\text{x}10^{-7}$ Ha/Bohr, which is consistent with previous observations. However, setting bond length to 1.5 Bohr results in significantly

high noncompliance between the analytical force and FD force, with 8.89x10^{-3} difference in forces. This dramatic change results from rapid change in occupation numbers for this mesh around this bond length as presented in Table 4.7.

Bond length [Bohr]	1st occupancy	2nd occupancy	3rd occupancy
1.49999	0.74777246575794	0.74777246575789	0.50445506849234
1.50000	0.74775165395487	0.74775165390007	0.50449669214085
1.50001	0.74773084010101	0.74773083990916	0.5045383199801

Table 4.7: Orbital occupations of Be_2 molecule - N3-8

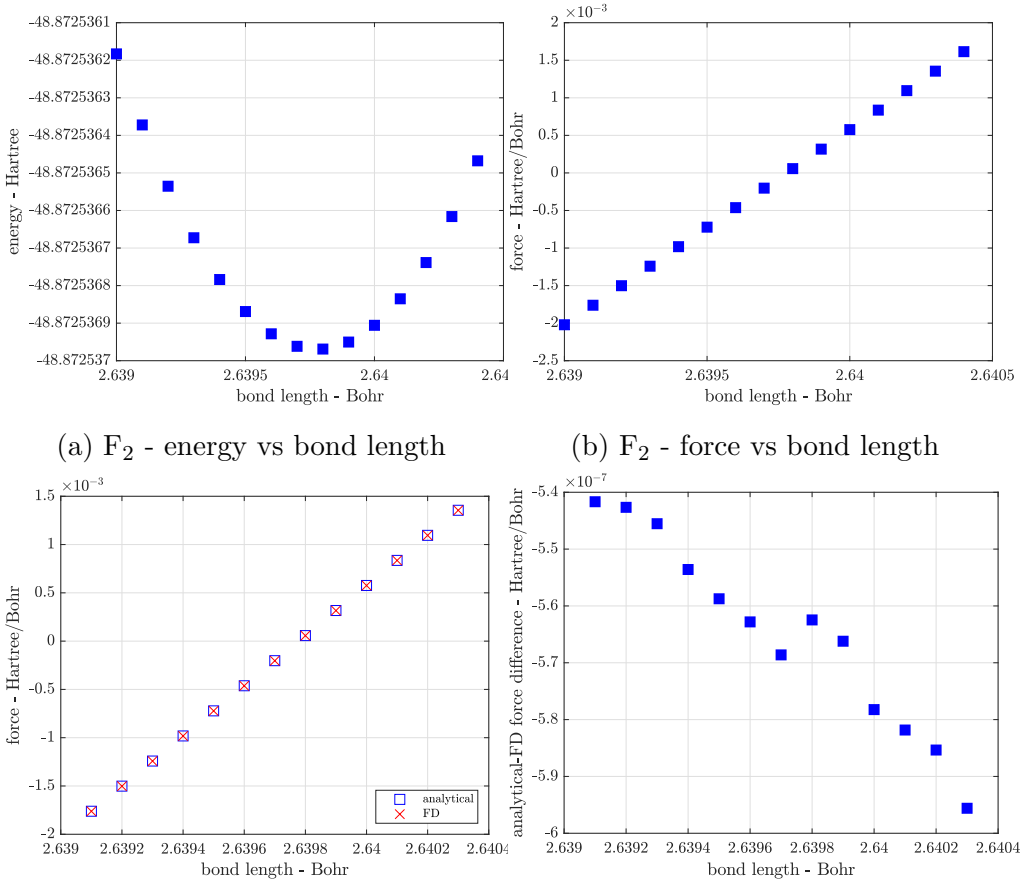

(a) F_2 - energy vs bond length

(b) F_2 - force vs bond length

(c) F_2 - force vs bond length

(d) F_2 - force difference vs bond length

Figure 4.10: Energy and force curves for F_2 around equilibrium - N3-16

If the same occupancy numbers are enforced for the unperturbed and perturbed cases (by setting perturbed occupancy numbers as in the unperturbed case), than analytical force and FD force are in compliance, with only a difference of $3.92\text{x}10^{-8}$. However, this does not conclude that analytical forces are calculated incorrectly without occupancy enforcement. When occupancy numbers change upon perturbation, entropy effects must be considered as well [44] in the following way:

$$2\sum_{i}^{N/2} f_i' \epsilon_i = S' \tag{4.2}$$

Therefore, an additional FD term is calculated using entropy values only in Table 4.8, and its result is compared with the large force difference $8.89\text{x}10^{-3}$. They are observed to cancel out each other to the 10^{-7} accuracy, which is in compliance with result for Be_2 of 2.0 Bohr bond length.

Bond length [Bohr]	Entropy contribution [Ha]	FD entropy force [Ha/Bohr]
1.49999	-0.003645291515938	
1.50000	-0.00364538049133982	$8.89\text{x}10^{-3}$
1.50001	-0.00364546945263501	

Table 4.8: Force due to entropy change on Be_2 molecule - N3-8

Finally, analytical force convergence is investigated upon mesh refinement for F_2 molecule with bond length of 2.0 Bohr. GGA+NLCC parameters are used. Results can be seen in Fig 4.11. Note that black bars indicate the chemical accuracy border. Solutions with 3^{rd} order Lagrange and 2^{nd} order NURBS basis have failed to reach the desired chemical accuracy, again showing the benefit of using higher-order basis functions. Also note that 3^{rd} order NURBS basis reaches chemical accuracy much faster than all other choices, in particular than even the 5^{th} order Lagrange basis.

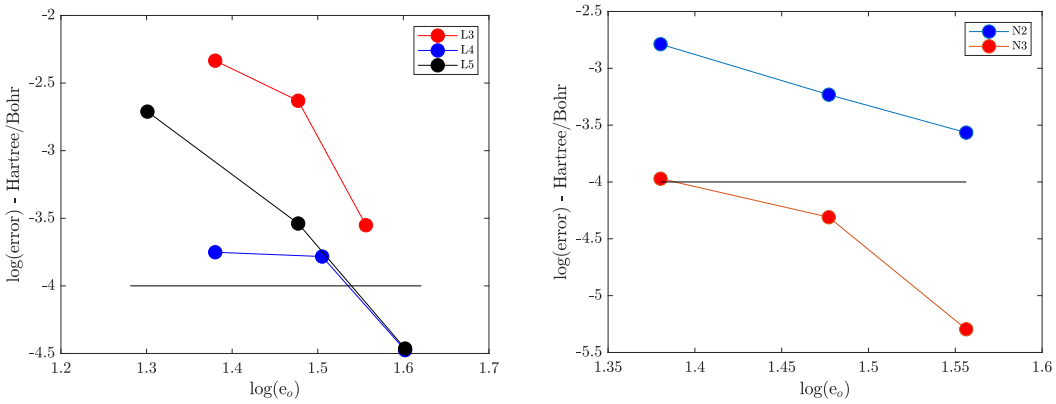

(a) F_2 - with L2, L3 and L5 basis

(b) F_2 - with N2 and N3 basis

Figure 4.11: Force convergence for F_2 upon mesh refinement

4.3 Five atom case

To demonstrate that analytical forces are variationally consistent at many-atom systems as well, force calculations on five atom molecules are conducted. First, for LDA assumption, a tetrahedral CH_4 molecule with a bond length of 2.08225 Bohr is perturbed along the x-axis. Coordinates of all atoms are described in Table 4.9.

Atom	x-coordinate [Bohr]	y-coordinate [Bohr]	z-coordinate [Bohr]
C	0.000000	0.000000	0.000000
H	-1.201888	-1.201888	-1.201888
H	1.201888	1.201888	-1.201888
H	-1.201888	1.201888	1.201888
H	1.201888	-1.201888	1.201888

Table 4.9: Atomic coordinates of CH_4 molecule - N3-16

Difference between the analytical force and FD force is calculated as 7.39×10^{-8} Ha/Bohr. Note that since H atoms are placed symmetrically, magnitude of the

force in each direction is the same for every H.

In order to demonstrate that symmetry is not required to obtain variationally consistent forces, tetrahedral geometry is broken by placing the first H atom at (-1.3,-1.4,-1.5). Then it is perturbed by $\Delta = 10^{-4}$ Bohr along each axis separately. Comparison of analytical and FD forces is displayed in Table 4.10.

	Analytical force [Ha/Bohr]	FD force [Ha/Bohr]	Difference [Ha/Bohr]
x-axis	0.035598575478	0.035598657976743	$2.85\text{x}10^{-8}$
y-axis	0.035883130414	0.035883085658149	$4.48\text{x}10^{-8}$
z-axis	0.045272970341	0.04527299282101	$2.24\text{x}10^{-8}$

Table 4.10: Force on non-tetrahedral CH_4 molecule - N3-16

Similarly, using GGA approximation with NLCC for an CF_4 molecule, one F atom is displaced out of the tetrahedral geometry to calculate forces. With a perturbation $\Delta = 10^{-4}$, FD forces on the displaced F atom are calculated. Comparison of the analytical and FD forces are displayed in Table 4.11.

	Analytical force [Ha/Bohr]	FD force [Ha/Bohr]	Difference [Ha/Bohr]
x-axis	-0.160565342291	-0.160566107608787	$7.65\text{x}10^{-7}$
y-axis	0.497825938033	0.49782531092675	$6.27\text{x}10^{-7}$
z-axis	-0.023819874644	-0.02382029293797	$4.18\text{x}10^{-7}$

Table 4.11: Force on non-tetrahedral CF_4 molecule - N3-16

Note that in all five atom molecule examples, force differences have been observed to be in integration error accuracy, which further verifies the variational consistency of the analytical forces.

4.4 Many atom case

Analytical force calculations have been conducted for C_{18} and C_{60} molecules using GGA+NLCC approximation. Since variational consistency has been established beyond doubt at this point, no finite difference analysis will be conducted for these molecules. Instead, analytical force results will be compared with reference values obtained using BigDFT [45] software. For both molecules, it is not viable to place the atoms symmetrically at each axis to nullify the egg-box effect. Therefore, calculations have been conducted at sufficiently refined meshes that are required for convergence to chemical accuracy. This is needed to judge the accuracy of the forces by checking the equivalence of their magnitude, as further discussed below.

C_{18} molecule is formed as polyyne structure [46] with radius 6.967 Bohr. Geometrically, every atom is expected to experience the same force magnitude. Therefore the mesh is refined until total analytical forces on atoms are consistent within a tolerance of at least $4.12\text{x}10^{-4}$ Ha/Bohr. Detailed results for each atom are shown in Fig. 4.12. Greatest total force difference with BigDFT is $8.11\text{x}10^{-4}$ Ha/Bohr. Note that BigDFT forces are at least $1.17\text{x}10^{-3}$ Ha/Bohr consistent with each other.

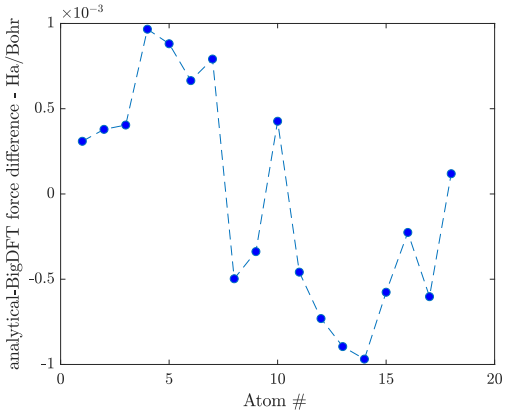

(a) C_{18} - force difference at x-axis

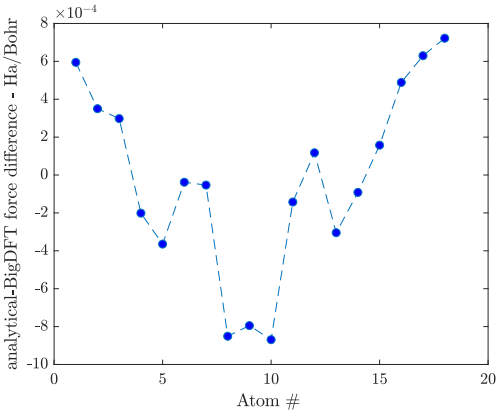

(b) C_{18} - force difference at y-axis

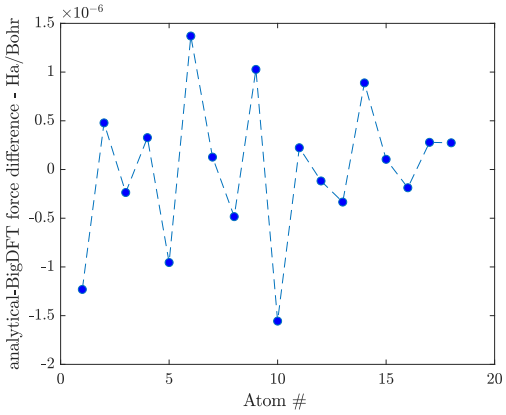

(c) C_{18} - force difference at z-axis

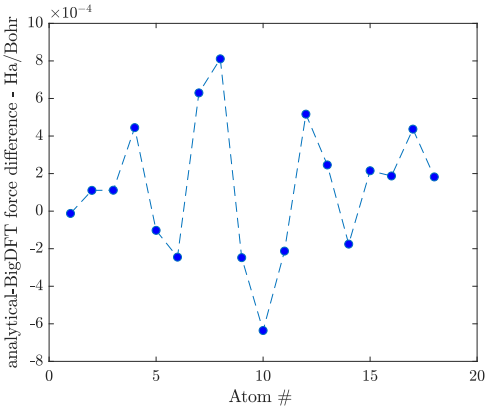

(d) C_{18} - total force difference

Figure 4.12: C_{18} - N3-52 - comparison of analytical forces with BigDFT forces

C_{60} molecule is formed as a buckyball structure [47]. Similarly, due to geometry every atom is again expected to experience the same force magnitude. Mesh is refined until total analytical forces on atoms are at least 5.65x10^{-5} Ha/Bohr consistent with each other. Detailed results for each atom are shown in Fig. 4.13. Greatest total force difference with BigDFT is 1.32x10^{-3} Ha/Bohr. Note that BigDFT forces are at least 1.18x10^{-3} Ha/Bohr consistent with each other. Since consistency in calculated forces for both C_{18} and C_{60} is better than that of BigDFT, calculated forces can be deduced to be more reliable.

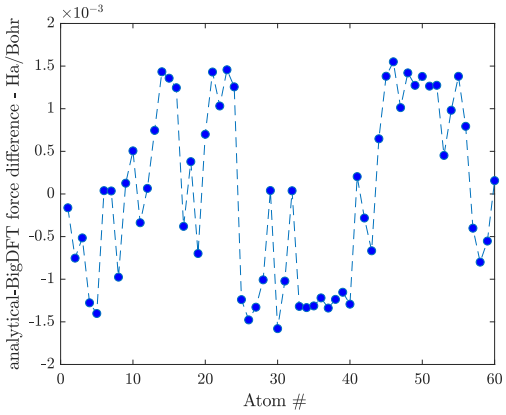

(a) C_{60} - force difference at x-axis

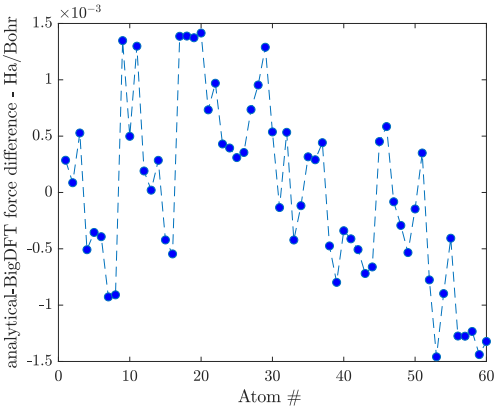

(b) C_{60} - force difference at y-axis

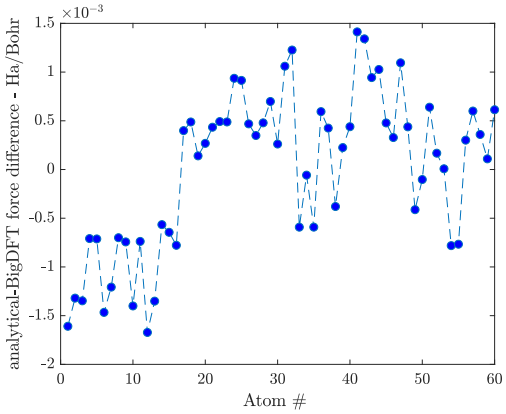

(c) C_{60} - force difference at z-axis

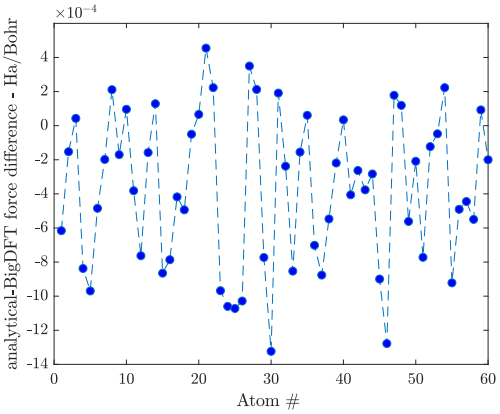

(d) C_{60}- total force difference

Figure 4.13: C_{60} - N3-52 - comparison of analytical forces with BigDFT forces

Chapter 5

All-electron force calculations

All-electron calculations have been conducted for single atom and two atom cases using LDA. Note that the main purpose of this section is to show that analytical forces calculated at all-electron setting are variationally consistent as well. Realistic geometry optimizations are not possible in the current mesh setup with all-electron forces, which will be commented upon.

5.1 Single atom case

Similar to the pseudopotential case, a single atom is placed at the center of the mesh. H atom is selected for this purpose. Single atom in vacuum is not expected to experience any force to within chemical accuracy even on relatively coarse meshes, which was the observation in pseudopotential calculations. However, this observation is not strictly valid for the all-electron case. Recall that a cusp formation must be represented at the atomic coordinate to properly resolve υ_{ext} in a discrete setting. For NURBS basis, this is achieved through decreasing the continuity of basis functions to C^0 at the atomic coordinate, and for Lagrange basis the atom must be placed at an element boundary where C^0 continuity naturally occurs. Recalling (3.13), discrete potentials calculated through Poisson

equations are used in all-electron force calculations. Therefore, discontinuity in the basis functions used to define these potentials causes a discontinuity in the analytical force as well, effectively also resulting with a non-zero force on the atom. This non-zero force is expected to decay to zero as the mesh is refined as shown in Fig 5.1.

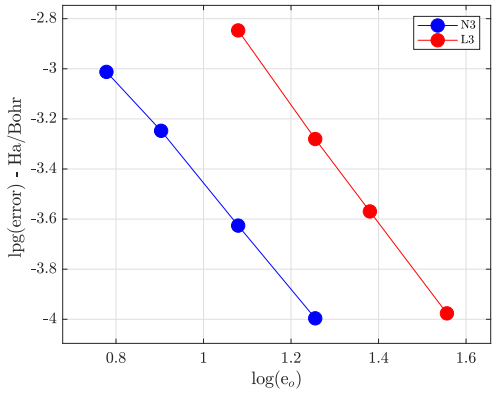

Figure 5.1: H - convergence of cusp induced force for 3$^{\text{rd}}$ order Lagrange and NURBS basis

Note that if a cusp is not formulated in mesh in NURBS basis, no force on the single atom is observed as expected, however this leads to considerable accuracy loss for energy. Furthermore, cusp induced force can be set zero by calculating the force at each adjacent element to the atomic coordinate, and then taking the mean of these forces. This way, discontinuity at each element border cancels out, resulting in zero force.

5.2 Two atom case

An H_2 molecule is chosen as the example. Arguing the variational consistency of forces in all-electron calculation is harder, as the finite difference test energies must be calculated at the same mesh. However, as the atoms are perturbed, cusps need to move as to construct the required C^0 continuity. Thus, finite difference test is conducted without the requirement that there must be a cusp

at the atomic coordinate. A sample test is presented in Table 5.1, by placing the atoms symmetrically at the mesh:

Bond length [Bohr]	Energy [Ha]	Analytical force [Ha/Bohr]	FD force [Ha/Bohr]	Difference [Ha/Bohr]
1.3448	-1.11917676481			
1.3458	-1.11917676481	0.0378864	0.0378866	$2.7\text{x}10^{-7}$
1.3468	-1.11925253817			

Table 5.1: Force on H_2 molecule - L3-12

Note that since Table 5.1 data is obtained with Lagrange basis, cusp induced forces are still observed along remaining Cartesian axis. An energy curve can still be set up by neglecting these forces. In Fig. 5.2, a cubic spline interpolation fit to energy-bond length curve is displayed, and its derivative is mapped to the bond length-force curve.

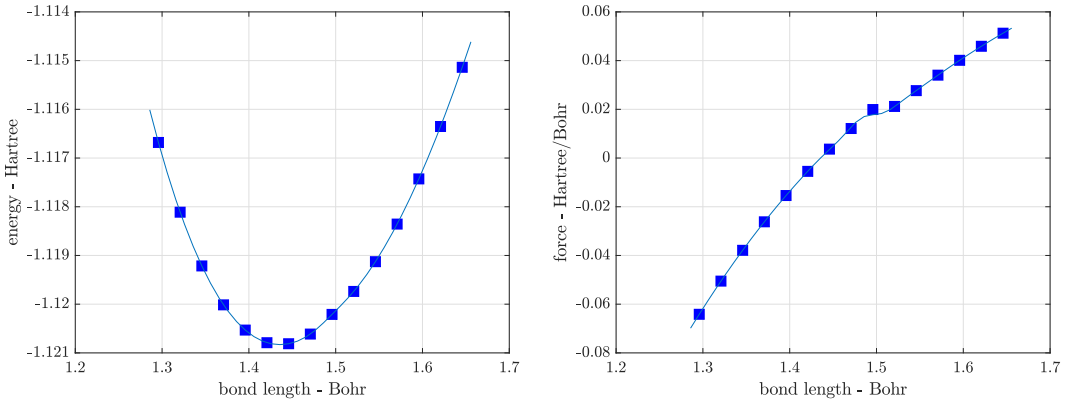

(a) H_2 - energy vs bond length (b) H_2 - force vs bond length

Figure 5.2: Energy and force curves for H_2 around equilibrium with fitting cubic spline interpolation - Derivative of energy curve is mapped to the force curve. - L3-12

Final remark regarding the all-electron force calculations is that egg-box effect is still relevant, in both energy and forces. To demonstrate this, an H_2 molecule with a bond length of 1.44 Bohr is translated by [0.014375,-0.0125,-0.001875]

Bohr at each step. Results are displayed in Fig. 5.3 and Fig. 5.4. Note that in both figures green lines represent the force magnitude that is expected for the respective setup if atoms were placed symmetrically in the mesh with no egg-box forces occurring.

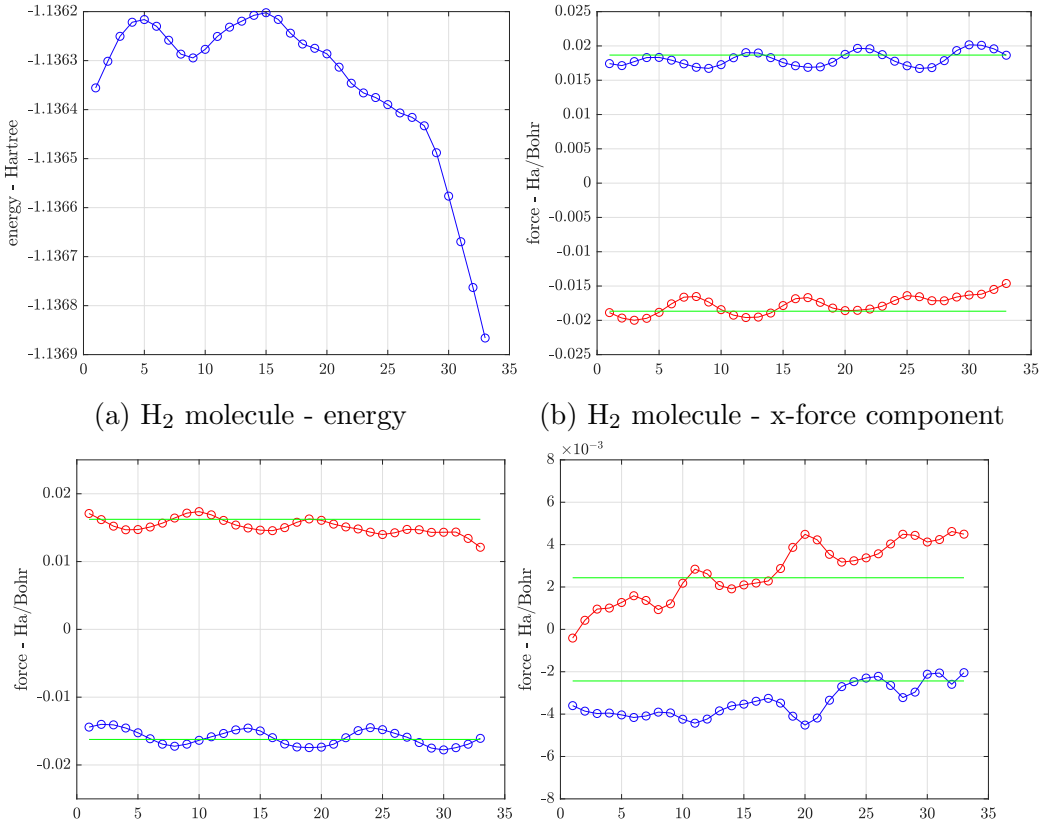

(a) H_2 molecule - energy

(b) H_2 molecule - x-force component

(c) H_2 molecule - y-force component

(d) H_2 molecule - z-force component

Figure 5.3: Eggbox effect for H_2 - N2-12 - each point is captured with a translation of [0.014375,-0.0125,-0.001875] Bohr with respect to the previous point

Note that the molecule is approaching to core patch border as it is translated. Steep increase in energy at final steps in both figures results from this. Also, for the Lagrange basis, the forces in x and y directions are observed to display sharp jump-like variations. These occur when the atoms change elements. Since the derivative of 2^{nd} order Lagrange polynomials have C^1 continuity only in the elements, but not across element boundaries, forces can suddenly change direction upon the atom entering a new element.

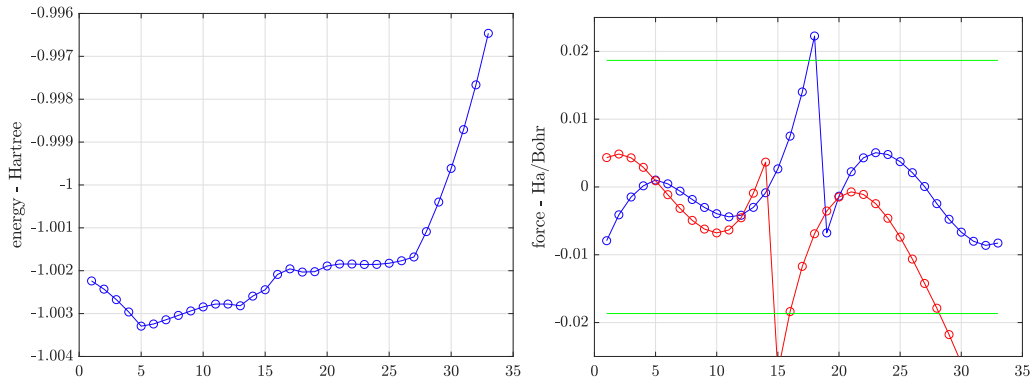

(a) H_2 molecule - energy

(b) H_2 molecule - x-force component

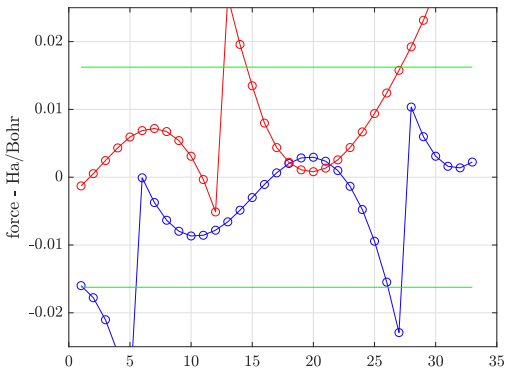

(c) H_2 molecule - y-force component

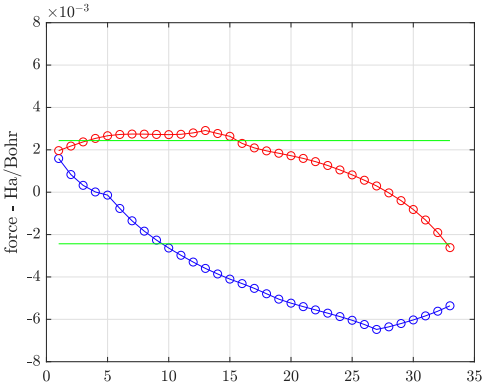

(d) H_2 molecule - z-force component

Figure 5.4: Eggbox effect for H_2 - L2-12 - each point is captured with a translation of [0.014375,-0.0125,-0.001875] Bohr with respect to the previous point

Chapter 6

Geometry optimization

Geometry optimization is conducted to find the ground state equilibrium geometries. Having variationally consistent forces allows geometry optimization at any mesh and basis setup, resulting with the corresponding equilibrium geometry.

6.1 Optimization algorithms

Before working on the actual FEM-formulated Kohn-Sham DFT problem, three algorithms are tested on two example problems. These three algorithms are conjugate gradient method, L-BFGS method, and FIRE method. Each method will be introduced briefly.

6.1.1 Conjugate gradient method

Conjugate gradient method (CG) [48] is a well-known method for solving linear systems of equations. Defining a function based on a quadratic form allows one to use CG for minima finding purposes. CG begins by moving in the gradient direction, and at each new iteration a different search direction is decided based

on the previous directions. Along each search direction, a line search is conducted to find the minima along that line. An outline of CG is given at (6.1).

1) $\boldsymbol{F} = -\nabla E(\boldsymbol{x})$

2) $\boldsymbol{d} = \boldsymbol{F}$ where $\boldsymbol{d}$ is the search direction.

3) Conduct line minimization along $\boldsymbol{d}$.

4) Move the system. Update $\boldsymbol{x}$.

5) $\boldsymbol{F} = -\nabla E(\boldsymbol{x})$

6) $\boldsymbol{d} = \boldsymbol{d} + \alpha \boldsymbol{F}$ where α is calculated using Polak-Ribiere method.

7) Move the system. Update $\boldsymbol{x}$.

8) Check convergence. If the system has not converged, return to the fifth step.

(6.1)

Ideally, CG is expected to converge in at at most n steps where n is the number of degrees of freedom in the system if the problem remains quadratic in nature. However, due to numerical errors, this is usually not the case. Moreover, line minimization method greatly affects the performance of CG. Some methods are very safe, almost guaranteeing convergence yet working very slowly, while some algorithms can be fast at the risk of nonconvergence. Two different methods will be considered in example problems.

Convergence criterion also requires consideration. Common choices include norm of gradient $\boldsymbol{F}$ and change in $\boldsymbol{x}$. For this work, $\boldsymbol{F}$ will be monitored for convergence because in the ground state geometry, the system is expected to experience no force.

6.1.2 Limited-memory Broyden–Fletcher–Goldfarb–Shanno method

Limited-memory Broyden–Fletcher–Goldfarb–Shanno, (L-BFGS) [49] is also a well-established algorithm, though unlike CG, L-BFGS uses Hessian matrix as well when deciding search directions. Currently, second derivative calculation is

not implemented for the DFT problem, however, this is no obstacle in using L-BFGS since this method does not calculate Hessian matrix exactly, but produces a estimate for it. An outline of L-BFGS is given at (6.2).

1) $\boldsymbol{F} = -\nabla E(\boldsymbol{x})$

2) Conduct an initial line minimization along. $\boldsymbol{F}$.

3) Record $\Delta\boldsymbol{F}$ and $\boldsymbol{\Delta x}$.

4) Use the last m $\Delta\boldsymbol{F}$ and $\boldsymbol{\Delta x}$ values to calculate the Hessian matrix.

5) Calculate $\boldsymbol{d}$ using the Hessian matrix.

6) Conduct line minimization along $\boldsymbol{d}$.

7) Move the system. Update $\boldsymbol{x}$.

8) Check convergence. If the system has not converged, return to the third step.

(6.2)

Value of m greatly affects the performance of algorithm. $m = 5$ is observed as the optimal value for most cases.

6.1.3 Fast inertial relaxation engine method

Fast inertial relaxation engine (FIRE) [50] is a novel method compared to CG and L-BFGS, taking its roots from molecular dynamics. At each iteration, the system is moved with a time integration scheme in a direction and with a magnitude set by FIRE. Movement of the system is accelerated as long as it is moving towards a minima, however if movement away from the minima occurs, system is frozen

and started again. An outline of FIRE is given at (6.3)

1) $\boldsymbol{F} = -\nabla E(\boldsymbol{x})$

2) Move the system using a molecular dynamics scheme.

3) Calculate power as $P = \boldsymbol{F}.\boldsymbol{v}$

4) $\boldsymbol{v} = (1-\alpha)\boldsymbol{v} + \alpha\dfrac{\boldsymbol{F}(t)}{|\mathbf{F}(t)|}|\boldsymbol{v}|, \quad \dot{\boldsymbol{v}} = \dfrac{\boldsymbol{F}(t)}{m} - \gamma(t)|\boldsymbol{v}(t)|[\dfrac{\boldsymbol{v}(t)}{|\boldsymbol{v}(t)|} - \dfrac{\boldsymbol{F}(t)}{|\boldsymbol{F}(t)|}]$

5) $\begin{cases} P > 0 \; and \; P > 0 \;\; \text{for } N_{min} \text{ steps }, & \Delta t = \min(\Delta t f_{inc}, \Delta t_{max}), \alpha = \alpha f_\alpha \\ P \leq 0, & \Delta t = \Delta t f_{dec}, \;\; \boldsymbol{v} = \mathbf{0}, \;\; \alpha = \alpha_{start} \end{cases}$

6) Check convergence. If the system has not converged, return to the first step. (6.3)

Unlike CG, it is not practical to use $\boldsymbol{x}$ as the convergence parameter since movement of the system depends on its current velocity. Therefore, FIRE iterations have to be continued until $\boldsymbol{F}$ satisfies a preset condition.

Suggested values [50] are used for N_{min}, f_{inc}, f_{dec}, α_{start} ve f_α parameters. Setting $m = 1$, Δt is kept as the only variable parameter. Two different time integration schemes will be tested, semi implicit Euler(SIM) and velocity-Verlet (VV).

6.2 Example problems

6.2.1 Spiral problem

Spiral problem is chosen as the first example in the comparison of geometry optimization algorithms. The aim is to reach to minima of the landscape constituted by (6.4):

$$f(r,\theta) = \sin(\pi r + \theta) + \frac{r^2}{10} \tag{6.4}$$

An exemplary optimization route is displayed in Fig. 6.1.

(a) spiral landscape - top view (b) spiral landscape - bottom view

Figure 6.1: Geometry optimization on spiral landscape. Each green dot is an iteration step, while the pink dot is the starting point.

As mentioned earlier, line search algorithms can drastically affect the performance of CG and L-BFGS. Two line search algorithms are used: linmin [51] and Wolfe-conditioned [49]. linmin algorithm acts after deciding the exact interval where the minima is located, whereas Wolfe-conditioned algorithm searches for a step size that is large enough to be meaningful to take while refraining from taking a step that might be too large . Comparison of different algorithms with their variations is presented in Table 6.1.

	FIRE (SIM)	FIRE (VV)	CG (linmin)	CG (Wolfe)	L-BFGS (linmin)	L-BFGS (Wolfe)
Iteration	178	187	1186	882	1136	473

Table 6.1: Comparison of optimization algorithms for spiral problem.

FIRE algorithm, regardless of time integration scheme, is considerably better than CG and L-BFGS. linmin line search method displayed similar results for both CG and L-BFGS, yet Wolfe-conditioned line search method performs better for both algorithms, especially for L-BFGS. It can be concluded that linmin line search method prefers to act safe by locating the minima interval at each step yet at a significant computational cost in performance. Based on the performance on

the spiral problem, FIRE method with both time integration schemes is chosen to be tested alongside Wolfe-conditioned L-BFGS in the next problem.

6.2.2 Face centered cubic (FCC)problem

Second example problem is chosen to represent the DFT problem closer, along with numerously more degrees of freedom. A face centered 3x3x3 cubic structure is constructed. During geometry optimization, atoms at top and bottom faces are kept stationary, while the other atoms are initially perturbed randomly by 5% in the Cartesin coordinates. Interaction between the atoms are modeled using Leonard-Jones potentials [52]. Comparison of the chosen algorithms is presented in Table 6.2.

	FIRE (SIM)	FIRE (VV)	L-BFGS (Wolfe)
Iteration	108	98	101

Table 6.2: Comparison of optimization algorithms for FCC problem

Again, FIRE algorithm is shown to be fastest, although its difference with L-BFGS is negligible. Nevertheless, FIRE algorithm is chosen to conduct geometry optimizations at Kohn-Sham DFT problem for its speed, robustness and ease of implementation. Number of tuning parameters for FIRE is only one, Δt, while the Wolfe-conditioned line search method for L-BFGS contains more concepts such as 'meaningful step size' or 'too large of a step' that may be vague and need to be tuned specifically for the problem. Besides, presence of methods such as linmin further indicates that the robustness of the Wolfe-Conditioned line search method is susceptible to tuning parameters. Finally, velocity-Verlet method is chosen as the time integration scheme, since it is a very conventional scheme used in molecular dynamics calculations with no significant computational cost compared to semi implicit-Euler.

6.3 Pseudopotential geometry optimizations

Geometry optimizations in pseudopotential formulation have been conducted using FIRE for five molecules, H_2 and CH_4 with LDA, F_2, CF_4 and C_{18} with GGA+NLCC approximation. For LDA, reference ground state molecule geometries are obtained via ABINIT. Except for C_{18}, initial geometry and coordinates of all molecules satisfy symmetry in mesh in all Cartesian axes.

To begin with, an exemplary optimization is conducted on L3-12 setup to demonstrate the behavior of FIRE. Iterations are continued until force on each atom is reduced below 5x10^{-6} Ha/Bohr, a value well below the chemical accuracy. Results can be seen in Fig. 6.2. Energy, along with force, decreases with each FIRE iteration. At FIRE iteration 7, starting Δt is causes the minima to be missed and is halved. However, with iteration 13, system begins to accelerate. Note that after iteration 6, energy and force are settled, and the algorithm is searching for the very low force converge criterion. After each FIRE iteration, wavefunctions and density distribution of the system is recorded to be used as initial guess for the next FIRE iteration. Therefore, number of SCF iterations at intermediate FIRE iterations is significantly less than that of initial configuration.

Equilibrium bond length of H_2 molecule is compared with the reference value, 1.44732 Bohr, obtained via ABINIT, reported to the given accuracy. Table 6.3 displays the behavior of calculated bond length as mesh is refined for 3^{rd} order NURBS basis. Note that forces are reduced below 5x10^{-6} Ha/Bohr. Although usually larger force tolerances are used [8], because of the simplicity of the model, it is possible to show that even very small force tolerances can be satisfied. Calculated bond lengths display systematic convergence to the reference value as the mesh is refined.

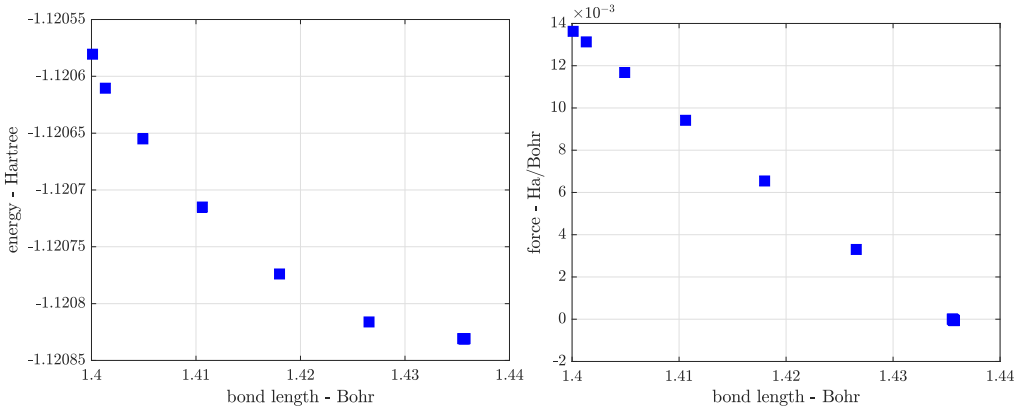

(a) energy vs bond length

(b) force vs bond length

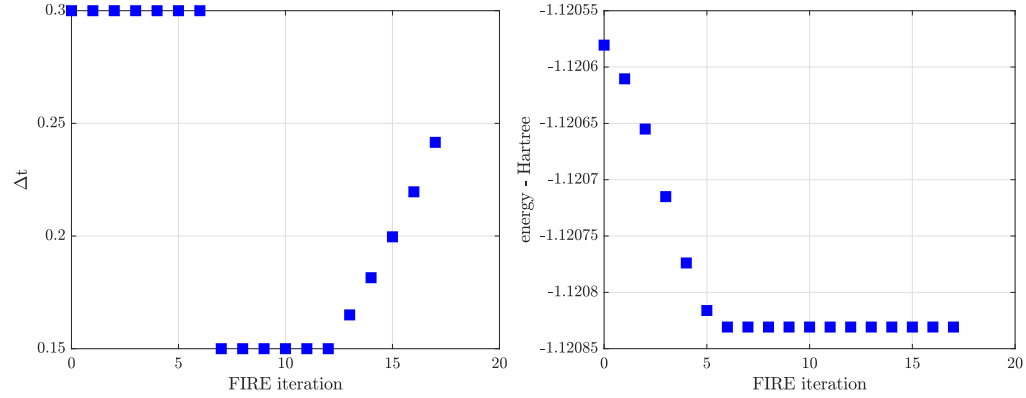

(c) time step vs FIRE iteration

(d) energy vs FIRE iteration

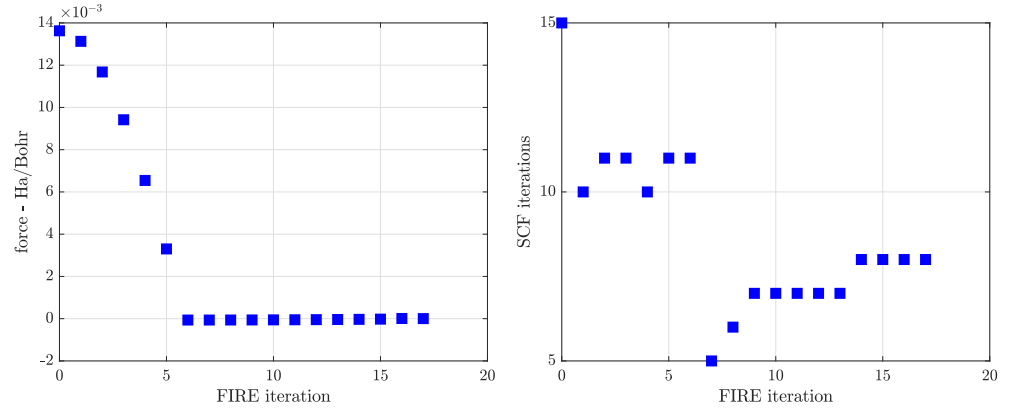

(e) force vs FIRE iteration

(f) SCF iteration vs FIRE iteration

Figure 6.2: Evolution of system and FIRE parameters throughout the optimization

	Optimized bond length [Bohr]	Diff. with reference [Bohr]	Diff. %
$e_0 = 8$	1.4828014	0.0354754	2.45
$e_0 = 12$	1.4279258	0.0194002	1.34
$e_0 = 16$	1.4550144	0.0076884	0.53
$e_0 = 24$	1.4483014	0.0009754	0.07
$e_0 = 36$	1.4473314	0.0000054	0.000373

Table 6.3: Optimized H-H bond length of H_2 molecule - N3

Also, equilibrium bond length of CH_4 molecule is also compared with the reference value, 2.07187 Bohr, obtained via ABINIT, reported to the given accuracy. Table 6.4 displays the systematic convergence trend for the calculated bond length as mesh is refined for 3^{rd} order NURBS basis. Note that forces are the reduced below 10^{-5} Ha/Bohr.

	Optimized bond length [Bohr]	Diff. with reference [Bohr]	Diff. %
$e_0 = 8$	2.0336263	0.038244	1.85
$e_0 = 12$	2.0460795	0.02579	1.24
$e_0 = 16$	2.0527415	0.0191295	0.92
$e_0 = 24$	2.074269	0.002397	0.12
$e_0 = 30$	2.0719214	0.0000503	0.0024

Table 6.4: Optimized C-H bond length of CH_4 molecule - N3

For F_2 and CF_4 molecules using GGA+NLCC assumption, force tolerance is kept at 10^{-5} Ha/Bohr. Using N3-30 setups, bond length of F_2 is calculated as 2.6746306 Bohr, whereas C-F bond length in CF_4 molecule has been optimized as 2.56632 Bohr.

Finally, as an example of geometry optimization on larger molecules, a C_{18} molecule initially in polyyne [46] structure with alternating bond length is relaxed. An N3-52 setup is used with 186021 degrees of freedom. Difference in

length between two types of bonds at polyyne geometry is 0.3080 Bohr. A force convergence tolerance of 10^{-4} Ha/Bohr is chosen due to the size of the problem. Optimized geometry is observed to be cumulene structure of the molecule, where each bond length is equal with the difference between the maximum and minimum bond lengths only as $4.4\text{x}10^{-4}$ Bohr. Finally, a 0.0623 Hartree decrease in energy is obtained going from polyyne to cumulene structure. Fig. 6.3 displays the initial and final density distributions in the optimization process. Optimized geometry is in agreement with previously conducted DFT calculations in literature [53], which suggest that DFT methods in the absence of high amount of exchange effects predict the ground state geometry of C_{18} to be in cumulene structure.

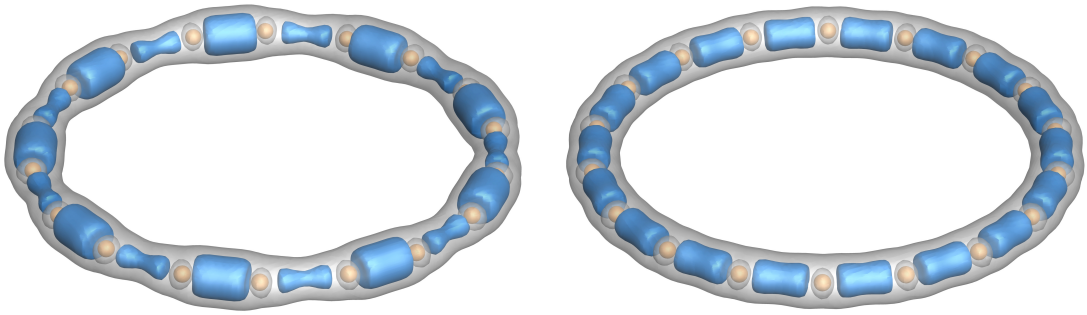

(a) initial polyyne structure (b) optimized cumulene structure

Figure 6.3: Density distribution of geometrically optimized C_{18} molecule

This example concludes the discussion of geometry optimizations. Currently implemented force calculations and geometry optimization algorithm are capable of finding the ground-state geometry of molecules as large as 18 atom systems.

Chapter 7

Conclusion

This work aimed to calculate variationally consistent atomic forces in a finite element based Kohn-Sham density functional framework with the end goal of utilizing these forces for molecular geometry optimization. Both NURBS meshes within isogeometric analysis concept and interpolatory Lagrange meshes are employed, although with a heavy emphasis on NURBS.

Starting with the Hellmann-Feynman theorem, variationally consistent force expressions are derived. Sample force calculations were first presented using pseudopotential setting. Egg-box effect was observed in the lack of symmetry in the placement of the molecule within the mesh. Magnitude of this effect was shown to diminish with improvements in the solution quality either by employing a higher order basis function or through mesh refinement by increasing the element numbers. Furthermore, using the finite difference method, variational accuracy of analytical forces was verified. Variety of examples are presented for both LDA and GGA+NLCC cases. Additionally, accuracy of analytical forces was further tested using reference values in the literature. Similar tests were conducted and similar results were observed for all-electron calculations as well.

Finally, geometry optimization was conducted. FIRE algorithm was chosen to implement in the Kohn-Sham DFT problem due to its computational efficiency,

robustness, and implementation ease. Geometry optimization was conducted for H_2 and CH_4 in LDA and F_2 and CF_4 in GGA+NLCC. LDA results were compared with reference values, showing as much as less than 0.001% discrepancy in calculated bond lengths. Systems as large as C_{18} can currently be handled by the presented computational framework.

Bibliography

[1] R. M. Martin, *Electronic Structure: Basic Theory and Practical Methods*. Cambridge University Press, 2004.

[2] A. Szabo and N. S. Ostlund, *Modern quantum chemistry: introduction to advanced electronic structure theory*. Courier Corporation, 2012.

[3] R. Parr, "Density-functional theory of atoms and molecules," 1989.

[4] W. Koch and M. C. Holthausen, *A chemist's guide to density functional theory*. John Wiley & Sons, 2015.

[5] L. Lin, J. Lu, and L. Ying, "Numerical methods for Kohn–Sham density functional theory," *Acta Numerica*, vol. 28, pp. 405–539, 2019.

[6] E. Tsuchida and M. Tsukada, "Electronic-structure calculations based on the finite-element method," *Physical Review B*, vol. 52, no. 8, p. 5573, 1995.

[7] J. Pask and P. Sterne, "Finite element methods in ab initio electronic structure calculations," *Modelling and Simulation in Materials Science and Engineering*, vol. 13, no. 3, p. R71, 2005.

[8] P. Motamarri, S. Das, S. Rudraraju, K. Ghosh, D. Davydov, and V. Gavini, "DFT-FE–a massively parallel adaptive finite-element code for large-scale density functional theory calculations," *Computer Physics Communications*, vol. 246, p. 106853, 2020.

[9] İ. Temizer, "Radial and three-dimensional nonlocal pseudopotential calculations in gradient-corrected Kohn-Sham density functional theory based on

higher-order finite element methods," *Computer Methods in Applied Mechanics and Engineering*, vol. 386, p. 114094, 12 2021.

[10] İ. Temizer, P. Motamarri, and V. Gavini, "NURBS-based non-periodic finite element framework for Kohn-Sham density functional theory calculations," *Journal of Computational Physics*, vol. 410, p. 109364, 02 2020.

[11] P. Motamarri, M. Nowak, K. Leiter, J. Knap, and V. Gavini, "Higher-order adaptive finite-element methods for Kohn–Sham density functional theory," *Journal of Computational Physics*, vol. 253, pp. 308–343, 2013.

[12] R. P. Feynman, "Forces in molecules," *Phys. Rev.*, vol. 56, pp. 340–343, Aug 1939.

[13] P. Pulay, "Ab initio calculation of force constants and equilibrium geometries in polyatomic molecules," *Molecular Physics*, vol. 17, no. 2, pp. 197–204, 1969.

[14] R. Yu, D. Singh, and H. Krakauer, "All-electron and pseudopotential force calculations using the linearized-augmented-plane-wave method," *Phys. Rev. B*, vol. 43, pp. 6411–6422, Mar 1991.

[15] J. M. Soler and A. R. Williams, "Simple formula for the atomic forces in the augmented-plane-wave method," *Physical Review B*, vol. 40, no. 3, p. 1560, 1989.

[16] J. E. Jaffe and A. C. Hess, "Gaussian basis density functional theory for systems periodic in two or three dimensions: Energy and forces," *The Journal of chemical physics*, vol. 105, no. 24, pp. 10983–10998, 1996.

[17] D. Porezag and M. R. Pederson, "Optimization of gaussian basis sets for density-functional calculations," *Physical Review A*, vol. 60, no. 4, p. 2840, 1999.

[18] J. VandeVondele, M. Krack, F. Mohamed, M. Parrinello, T. Chassaing, and J. Hutter, "Quickstep: Fast and accurate density functional calculations using a mixed Gaussian and plane waves approach," *Comput. Phys. Commun.*, vol. 167, pp. 103–128, 2005.

[19] G. Lippert, J. Hutter, and M. Parrinello, "The Gaussian and augmented-plane-wave density functional method for ab initio molecular dynamics simulations," *Theoretical Chemistry Accounts*, vol. 103, no. 2, pp. 124–140, 1999.

[20] S. Ghosh and P. Suryanarayana, "Higher-order finite-difference formulation of periodic orbital-free density functional theory," *Journal of Computational Physics*, vol. 307, pp. 634–652, 2016.

[21] S. Ghosh and P. Suryanarayana, "SPARC: Accurate and efficient finite-difference formulation and parallel implementation of density functional theory: Isolated clusters," *Computer Physics Communications*, vol. 212, pp. 189–204, 2017.

[22] G. Zhang, L. Lin, W. Hu, C. Yang, and J. E. Pask, "Adaptive local basis set for Kohn–Sham density functional theory in a discontinuous Galerkin framework ii: Force, vibration, and molecular dynamics calculations," *Journal of Computational Physics*, vol. 335, pp. 426–443, 2017.

[23] P. Suryanarayana, V. Gavini, T. Blesgen, K. Bhattacharya, and M. Ortiz, "Non-periodic finite-element formulation of Kohn–Sham density functional theory," *Journal of the Mechanics and Physics of Solids*, vol. 58, no. 2, pp. 256–280, 2010.

[24] P. Motamarri and V. Gavini, "Configurational forces in electronic structure calculations using Kohn-Sham density functional theory," *Physical Review B*, vol. 97, no. 16, p. 165132, 2018.

[25] P. Motamarri, *Large-scale real-space Kohn-Sham density functional theory calculations using adaptive finite-element discretization*. PhD thesis, University of Michigan, 2014.

[26] E. Artacho, E. Anglada, O. Diéguez, J. D. Gale, A. García, J. Junquera, R. M. Martin, P. Ordejón, J. M. Pruneda, D. Sánchez-Portal, *et al.*, "The SIESTA method; developments and applicability," *Journal of Physics: Condensed Matter*, vol. 20, no. 6, p. 064208, 2008.

[27] X. Andrade, D. A. Strubbe, U. de Giovannini, A. H. Larsen, M. J. T. Oliveira, J. Alberdi-Rodriguez, A. Varas, I. Theophilou, N. Helbig, M. Verstraete, L. Stella, F. Nogueira, A. Aspuru-Guzik, A. Castro, M. Marques, and Á. Rubio, "Real-space grids and the Octopus code as tools for the development of new simulation approaches for electronic systems.," *Physical chemistry chemical physics : PCCP*, vol. 17 47, pp. 31371–96, 2015.

[28] T. Ono, M. Heide, N. Atodiresei, P. Baumeister, S. Tsukamoto, and S. Blügel, "Real-space electronic structure calculations with full-potential all-electron precision for transition metals," *Physical Review B*, vol. 82, no. 20, p. 205115, 2010.

[29] N. D. Hine, M. Robinson, P. D. Haynes, C.-K. Skylaris, M. C. Payne, and A. A. Mostofi, "Accurate ionic forces and geometry optimization in linear-scaling density-functional theory with local orbitals," *Physical Review B*, vol. 83, no. 19, p. 195102, 2011.

[30] E. Tsuchida, Y.-K. Choe, and T. Ohkubo, "An adaptive finite-element method for large-scale ab initio molecular dynamics simulations," *Physical Chemistry Chemical Physics*, vol. 17, no. 47, pp. 31444–31452, 2015.

[31] M. Novák, J. Vackář, and R. Cimrman, "Evaluating Hellmann–Feynman forces within non-local pseudopotentials," *Computer Physics Communications*, vol. 250, p. 107034, 2020.

[32] D. J. Griffiths and D. F. Schroeter, *Introduction to quantum mechanics*. Cambridge University Press, 2018.

[33] P. Hohenberg and W. Kohn, "Inhomogeneous electron gas," *Phys. Rev.*, vol. 136, pp. B864–B871, Nov 1964.

[34] M. Levy, "Electron densities in search of hamiltonians," *Phys. Rev. A*, vol. 26, pp. 1200–1208, Sep 1982.

[35] W. Kohn and L. J. Sham, "Self-consistent equations including exchange and correlation effects," *Phys. Rev.*, vol. 140, pp. A1133–A1138, Nov 1965.

[36] W. E. Pickett, "Pseudopotential methods in condensed matter applications," *Computer Physics Reports*, vol. 9, no. 3, pp. 115–197, 1989.

[37] C. Hartwigsen, S. Goedecker, and J. Hutter, "Relativistic separable dual-space Gaussian pseudopotentials from h to rn," *Phys. Rev. B*, vol. 58, pp. 3641–3662, Aug 1998.

[38] D. J N Reddy, *An Introduction to the Finite Element Method*. McGraw-Hill Education, 2005.

[39] Y. Zhou, Y. Saad, M. L. Tiago, and J. R. Chelikowsky, "Self-consistent-field calculations using Chebyshev-filtered subspace iteration," *Journal of Computational Physics*, vol. 219, no. 1, pp. 172–184, 2006.

[40] L. Piegl and W. Tiller, *The NURBS Book*. New York, NY, USA: Springer-Verlag, second ed., 1996.

[41] J. A. Cottrell, T. J. Hughes, and Y. Bazilevs, *Isogeometric analysis: toward integration of CAD and FEA*. John Wiley & Sons, 2009.

[42] J. C. Strikwerda, *Finite difference schemes and partial differential equations*. SIAM, 2004.

[43] X. Gonze, B. Amadon, P.-M. Anglade, J.-M. Beuken, F. Bottin, P. Boulanger, F. Bruneval, D. Caliste, R. Caracas, M. Côté, *et al.*, "ABINIT: First-principles approach to material and nanosystem properties," *Computer Physics Communications*, vol. 180, no. 12, pp. 2582–2615, 2009.

[44] M. Weinert and J. W. Davenport, "Fractional occupations and density-functional energies and forces," *Phys. Rev. B*, vol. 45, pp. 13709–13712, Jun 1992.

[45] L. Genovese, A. Neelov, S. Goedecker, T. Deutsch, S. A. Ghasemi, A. Willand, D. Caliste, O. Zilberberg, M. Rayson, A. Bergman, *et al.*, "Daubechies wavelets as a basis set for density functional pseudopotential calculations," *The Journal of chemical physics*, vol. 129, no. 1, p. 014109, 2008.

[46] G. V. Baryshnikov, R. R. Valiev, A. V. Kuklin, D. Sundholm, and H. Ågren, "Cyclo [18] carbon: Insight into electronic structure, aromaticity, and surface coupling," *The journal of physical chemistry letters*, vol. 10, no. 21, pp. 6701–6705, 2019.

[47] P. Senn, "Computation of the cartesian coordinates of buckminsterfullerene," *Journal of chemical education*, vol. 72, no. 4, p. 302, 1995.

[48] J. R. Shewchuk *et al.*, "An introduction to the conjugate gradient method without the agonizing pain," 1994.

[49] J. Nocedal and S. Wright, *Numerical optimization*. Springer Science & Business Media, 2006.

[50] E. Bitzek, P. Koskinen, F. Gähler, M. Moseler, and P. Gumbsch, "Structural relaxation made simple," *Physical review letters*, vol. 97, no. 17, p. 170201, 2006.

[51] W. H. Press, S. A. Teukolsky, W. T. Vetterling, and B. P. Flannery, *Numerical Recipes in FORTRAN; The Art of Scientific Computing*. USA: Cambridge University Press, 2nd ed., 1993.

[52] X. Wang, S. Ramírez-Hinestrosa, J. Dobnikar, and D. Frenkel, "The Lennard-Jones potential: when (not) to use it," *Physical Chemistry Chemical Physics*, vol. 22, no. 19, pp. 10624–10633, 2020.

[53] A. J. Stasyuk, O. A. Stasyuk, M. Solà, and A. A. Voityuk, "Cyclo[18]carbon: the smallest all-carbon electron acceptor," *Chem. Commun.*, vol. 56, pp. 352–355, 2020.

Appendix A

Pseupotential force calculations

Fourth order central finite difference method predicts the force as

$$F_A(\mathbf{R}) = \frac{E(\mathbf{R}-2\Delta) - 8E(\mathbf{R}-\Delta) + 8E(\mathbf{R}+\Delta) - E(\mathbf{R}-2\Delta)}{12\Delta} \qquad \text{(A.1)}$$

with the leading error term $\sim \Delta^4 E^{(5)}$.

Bond length [Bohr]	Energy [Ha]	Analytical force [Ha/Bohr]	FD force [Ha/Bohr]	Difference [Ha/Bohr]
1.99998	-1.0800637891950711			
1.99999	-1.0800607343300250			
2.00000	-1.0800576794512646	0.305488559949	0.305488559235	0.3054885593118
2.00001	-1.0800546245588403			
2.00002	-1.0800515696527107			

Table A.1: Force on H_2 molecule - N3-8

Absolute difference between the 2^{nd} and 4^{th} FD forces are 7.6x10^{-11}, therefore for this particular example 2^{nd} is deemed to be 10^{-10} accurate.